Available online at www.eccomasproceedia.org
Eccomas Proceedia COMPDYN (2021) 2033-2057

ECCOMAS
Proceedia

COMPDYN 2021
8th ECCOMAS Thematic Conference on
Computational Methods in Structural Dynamics and Earthquake Engineering
M. Papadrakakis, M. Fragiadakis (eds.)
Streamed from Athens, Greece, 28 - 30 June 2021

ENRICHED BEAM FINITE ELEMENT MODELS WITH TORSION AND SHEAR WARPING FOR DYNAMIC ANALYSIS OF FRAME STRUCTURES

Daniela Addessi, Paolo Di Re and Cristina Gatta

Department of Structural and Geotechnical Engineering, Sapienza University of Rome
via Eudossiana 18, 00184, Rome, Italy
e-mail: {daniela.addessi,paolo.dire,cristina.gatta}@uniroma1.it

Abstract. *This work investigates the performance of the enhanced beam Finite Element (FE) formulations proposed in [20] for the dynamic response of frame structures subjected to shear and torsional actions. These formulations introduce enriched kinematic descriptions to describe the out-of-plane deformations of beam cross-sections, in addition to the standard in-plane rigid modes. First model is based on the Vlasov's theory, enriched to include shear induced warping, and is developed according to a displacement-based approach. To this end, additional degrees of freedom (DOFs) are introduced at the two element end nodes and are used to interpolate warping along the element axis, so that the influence of warping restraints at the element boundaries are properly accounted for. Second model is based on the Benscoter's warping theory, also enriched to include shear warping, and is developed according to a mixed formulation free from shear-locking. Third model is the extension of second formulation and considers a general and accurate warping description. Indeed, a variable number of additional DOFs is introduced over the element cross-section and the warping displacement field is interpolated at two levels, along the beam axis and over the cross-section plane.*

Numerical analyses are presented to assess the performances of the three models in describing the seismic response of frame structures, when shear/torsional actions dominate the structural behavior. Results are compared with the solutions obtained from standard beam and more involving shell and brick FE models.

Keywords: Seismic assessment, Dynamic analysis, Shear and torsion, Warping, Beam Finite Element.

ISSN:2623-3347
Peer-review under responsibility of the organizing committee of COMPDYN 2021.
doi:10.7712/120121.8621.19293

1 INTRODUCTION

Simulation of the mechanical behavior of large scale structures is a challenging task, although significant advances in computer technology were made during the last decades and increasingly accurate computational models were proposed. In particular, civil engineering structures subjected to seismic actions deserve special efforts, as the dynamic response to ground motions is strongly influenced by the material complex nonlinear behavior and multi-axial stress interaction. Many works have focused on the effects of in-plane and out-of plane cross-section deformation modes due to shear and torsional actions and, by employing enhanced beam models, they have proved that these phenomena can significantly reduce the element stiffness, influencing the natural frequencies of the structure [1] and producing local and global buckling under both static [2, 3, 4] and dynamic loading conditions [5]. Despite their considerable accuracy, full generalization of these models and their introduction in numerical codes for the analysis of large scale structures is hard to accomplish. Hence, more demanding two-dimensional (2D) plate/shell or three-dimensional (3D) Finite Element (FE) approaches are often used, although their lower efficiency and high computational cost. The adoption of beam FEs is to now the most convenient choice for the analysis of large scale framed structures. However, standard models are often based on classical rigid cross-section assumption and fail in correctly reproducing the structural response, even more when thin-walled members subjected to shear and torsion are considered.

Starting from the first proposals by Vlasov [6] and Benscoter [7], several enhanced beam theories and numerical models were presented [8, 9, 10, 11]. An extensive review of the first proposals is reported in [12], while more sophisticated formulations were recently developed, to include also effects due to shear forces, e.g. [13, 14, 15, 16, 17, 18]. However, only in few cases these models were focused on the analysis of large structures under dynamic loading conditions, e.g [19].

This work explores the application to dynamic field of the 3D beam FE formulations presented in [20] and originally developed for the static analysis of frame structures subjected to shear and torsional actions. Enriched kinematic descriptions are considered to include out-of-plane deformations of beam cross-sections, in addition to the classical in-plane rigid modes. Hence, warping effects related to both torsion and shear are accounted for.

First model is based on an extended Vlasov's theory that includes both torsional and shear warping and relies on an enriched displacement-based approach that prevents shear-locking [21]. The out-of-plane cross-section displacement field is assumed as the linear combination of three warping functions, a priori defined over the element cross-section, and the generalized cross-section torsional curvature and shear strains. By introducing additional degrees of freedom (DOFs) at the element end nodes, these generalized strains are interpolated along the axis as parabolic and linear functions, respectively. The model is referred to as Enhanced Vlasov Displacement-based Element (EVDE).

Second model is based on Benscoter's warping theory, also enriched to include both torsional and shear warping. As opposed to the first model, warping variables defined along the axis are assumed as independent kinematic quantities from cross-section strains. Hence, a mixed approach is followed, where the warping displacement field is interpolated along the element, together with the generalized cross-section stresses. The model is referred to as Simplified Warping Mixed Element (SWME).

Third model is the general extension of the above latter formulation. Indeed, in addition to the warping displacement interpolation along the element axis, this considers a 2D interpolation

1 INTRODUCTION

Simulation of the mechanical behavior of large scale structures is a challenging task, although significant advances in computer technology were made during the last decades and increasingly accurate computational models were proposed. In particular, civil engineering structures subjected to seismic actions deserve special efforts, as the dynamic response to ground motions is strongly influenced by the material complex nonlinear behavior and multi-axial stress interaction. Many works have focused on the effects of in-plane and out-of plane cross-section deformation modes due to shear and torsional actions and, by employing enhanced beam models, they have proved that these phenomena can significantly reduce the element stiffness, influencing the natural frequencies of the structure [1] and producing local and global buckling under both static [2, 3, 4] and dynamic loading conditions [5]. Despite their considerable accuracy, full generalization of these models and their introduction in numerical codes for the analysis of large scale structures is hard to accomplish. Hence, more demanding two-dimensional (2D) plate/shell or three-dimensional (3D) Finite Element (FE) approaches are often used, although their lower efficiency and high computational cost. The adoption of beam FEs is to now the most convenient choice for the analysis of large scale framed structures. However, standard models are often based on classical rigid cross-section assumption and fail in correctly reproducing the structural response, even more when thin-walled members subjected to shear and torsion are considered.

Starting from the first proposals by Vlasov [6] and Benscoter [7], several enhanced beam theories and numerical models were presented [8, 9, 10, 11]. An extensive review of the first proposals is reported in [12], while more sophisticated formulations were recently developed, to include also effects due to shear forces, e.g. [13, 14, 15, 16, 17, 18]. However, only in few cases these models were focused on the analysis of large structures under dynamic loading conditions, e.g [19].

This work explores the application to dynamic field of the 3D beam FE formulations presented in [20] and originally developed for the static analysis of frame structures subjected to shear and torsional actions. Enriched kinematic descriptions are considered to include out-of-plane deformations of beam cross-sections, in addition to the classical in-plane rigid modes. Hence, warping effects related to both torsion and shear are accounted for.

First model is based on an extended Vlasov's theory that includes both torsional and shear warping and relies on an enriched displacement-based approach that prevents shear-locking [21]. The out-of-plane cross-section displacement field is assumed as the linear combination of three warping functions, a priori defined over the element cross-section, and the generalized cross-section torsional curvature and shear strains. By introducing additional degrees of freedom (DOFs) at the element end nodes, these generalized strains are interpolated along the axis as parabolic and linear functions, respectively. The model is referred to as Enhanced Vlasov Displacement-based Element (EVDE).

Second model is based on Benscoter's warping theory, also enriched to include both torsional and shear warping. As opposed to the first model, warping variables defined along the axis are assumed as independent kinematic quantities from cross-section strains. Hence, a mixed approach is followed, where the warping displacement field is interpolated along the element, together with the generalized cross-section stresses. The model is referred to as Simplified Warping Mixed Element (SWME).

Third model is the general extension of the above latter formulation. Indeed, in addition to the warping displacement interpolation along the element axis, this considers a 2D interpolation

over the cross-section plane, thus allowing for higher order descriptions of the out-of-plane deformations and full coupling of all stress components. The model is referred to as Enhanced Warping Mixed Element (EWME).

Main details of the adopted beam FE models are reviewed, discussing their extension to dynamic field. For EVDE and EWME, detailed derivation of the element governing equations under dynamic effects is reported in [22] and [23], respectively, and is briefly recalled here. More focus is dedicated to the dynamic extension of SWME, which is presented as a simplified case of that proposed for the EWME.

Numerical analyses on a steel L frame and a reinforced concrete (RC) shear wall are presented to assess the performances of the three models in describing the seismic response of the structures, when shear/torsional actions dominate the structural behavior. Elasto-plastic and plastic-damage nonlinear material behavior is considered. Results are compared with the solutions obtained from standard beam and more involving shell and brick FE models.

2 BEAM FINITE ELEMENT FORMULATIONS

The adopted model formulations are described referring to a straight beam with the local intrinsic reference system (x, y, z) , being x the axis parallel to the section centroid locus and y and z two general orthogonal axes lying on the cross-section plane. The element length and the 2D domain of the cross-section are indicated as L and $A(x)$, respectively.

Under the assumption of small displacements and strains, all models introduce the description of the out-of-plane deformations partially removing the classical hypothesis of rigid cross-sections. Hence, displacements $\mathbf{u}_m(x, y, z)$ of the generic point *m* are defined as the sum of cross-section rigid body motions, $\mathbf{u}_r(x, y, z)$, and warping displacements, $\mathbf{u}_w(x, y, z)$, i.e.:

$$\mathbf{u}_m(x, y, z) = \mathbf{u}_r(x, y, z) + \mathbf{u}_w(x, y, z) = \begin{Bmatrix} u_r(x, y, z) \\ v_r(x, y, z) \\ w_r(x, y, z) \end{Bmatrix} + \begin{Bmatrix} u_w(x, y, z) \\ 0 \\ 0 \end{Bmatrix} \tag{1}$$

Accordingly, three non-zero strain components are introduced, that is the axial elongation $\varepsilon_{xx}(x, y, z)$ and the two transverse shear strains, $\gamma_{xy}(x, y, z)$ and $\gamma_{xz}(x, y, z)$. These are collected in vector $\boldsymbol{\varepsilon}_m(x, y, z)$ and are work-conjugate to the axial, $\sigma_{xx}(x, y, z)$, and shear stresses in the cross-section plane, $\tau_{xy}(x, y, z)$ and $\tau_{xz}(x, y, z)$, collected in vector $\boldsymbol{\sigma}_m(x, y, z)$.

Based on the above assumptions, three enriched beam FE formulations are derived. These are presented in detail in [20] and are summarized in the following, focusing the attention on the warping description hypotheses and the derivation of the element governing equations including inertia effects.

2.1 Enhanced Vlasov Displacement-based Element (EVDE)

The EVDE formulation considers nine DOFs at each of the two end nodes, i and j, of the element, being these the six standard translations and rotations, collected in vectors $\mathbf{u}_{i/j}$ and $\boldsymbol{\theta}_{i/j}$, respectively, and three additional DOFs used to describe cross-section warping, i.e. the end cross-section torsional curvature, $\chi_{xi/j}$, and shear strains, $\gamma_{yi/j}$ and $\gamma_{zi/j}$, collected in vectors $\boldsymbol{\eta}_i = \begin{Bmatrix} \chi_{x\,i} & \gamma_{y\,i} & \gamma_{z\,i} \end{Bmatrix}^T$ and $\boldsymbol{\eta}_j = \begin{Bmatrix} \chi_{x\,j} & \gamma_{y\,j} & \gamma_{z\,j} \end{Bmatrix}^T$ (Figure 1). Hence, the nodal displacement vector is written as:

$$\hat{\mathbf{u}} = \begin{Bmatrix} \mathbf{u}^T & \boldsymbol{\eta}^T \end{Bmatrix}^T = \begin{Bmatrix} \mathbf{u}_i^T & \boldsymbol{\theta}_i^T & \mathbf{u}_j^T & \boldsymbol{\theta}_j^T & \boldsymbol{\eta}_i^T & \boldsymbol{\eta}_j^T \end{Bmatrix}^T \tag{2}$$

vectors $\mathbf{u}^T$ and $\boldsymbol{\eta}^T$ collecting the standard and warping DOFs, respectively.

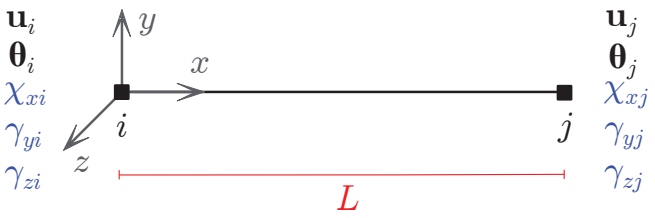

Figure 1: Standard (black) and warping (blue) nodal DOFs for the EVDE

A reference basic configuration is introduced to remove the element rigid body motions and only twelve basic displacements are used to define the element behavior. These are listed in vector $\hat{\mathbf{v}}$, that results as:

$$\hat{\mathbf{v}} = \begin{Bmatrix} u_j & \theta_{zi} & \theta_{zj} & \theta_{xj} & \theta_{yi} & \theta_{yj} & \chi_{xi} & \gamma_{yi} & \gamma_{zi} & \chi_{xj} & \gamma_{yj} & \gamma_{zj} \end{Bmatrix}^T = \hat{\mathbf{a}}_v \, \hat{\mathbf{u}} \tag{3}$$

being $\hat{\mathbf{a}}_v$ the kinematic operator that removes the rigid body motions [20].

To avoid shear locking issues, generalized cross-section displacement interpolation is performed by assuming the two cross-section shear strain fields, $\gamma_y(x)$ and $\gamma_z(x)$, as independent quantities, instead of the bending rotations, $\theta_y(x)$ and $\theta_z(x)$ [21]. Thus, cross-section kinematic vector results as:

$$\hat{\mathbf{u}}_s(x) = \begin{Bmatrix} u(x) & v(x) & \theta_x(x) & w(x) & \gamma_y(x) & \gamma_z(x) \end{Bmatrix}^T \tag{4}$$

being $u(x)$, $v(x)$ and $w(x)$ the rigid traslations and $\theta_x(x)$ the rigid torsional rotation. The nodal DOFs introduced permit to express the displacement fields $u(x)$, $\gamma_y(x)$ and $\gamma_z(x)$ as linear functions along the element axis, and $v(x)$, $w(x)$ and $\theta_x(x)$ as cubic polynomials. The relations between $\hat{\mathbf{u}}_s(x)$ and $\hat{\mathbf{v}}$ is written in compact form as:

$$\hat{\mathbf{u}}_s(x) = \hat{\mathbf{N}}(x) \, \hat{\mathbf{v}} \tag{5}$$

where $\hat{\mathbf{N}}(x)$ is the element shape function matrix containing the polynomial interpolations for the displacement and shear strain fields [20].

By enforcing the cross-section compatibility conditions, the generalized cross-section strain vector, $\hat{\mathbf{e}}(x) = \mathbf{D}(x) \, \hat{\mathbf{u}}_s(x)$, is introduced, being $\mathbf{D}(x)$ the compatibility differential operator. Vector $\hat{\mathbf{e}}(x)$ collects the axial strain, $\varepsilon_G(x)$, flexural curvatures, $\chi_z(x)$ and $\chi_y(x)$, torsional curvature, $\chi_x(x)$, shear strains, $\gamma_y(x)$ and $\gamma_z(x)$, and additional warping strains, $\zeta_x(x) = \chi_x'(x)$, $\zeta_y(x) = \gamma_y'(x)$, $\zeta_z(x) = \gamma_z'(x)$, related to warping, i.e.:

$$\hat{\mathbf{e}}(x) = \begin{Bmatrix} \varepsilon_G(x) & \chi_z(x) & \gamma_y(x) & \chi_x(x) & \chi_y(x) & \gamma_z(x) & \zeta_x(x) & \zeta_y(x) & \zeta_z(x) \end{Bmatrix}^T \tag{6}$$

where the apex denotes the derivative with respect to x. Hence, the following relationship holds between the generalized cross-section strains and the nodal basic displacement vector:

$$\hat{\mathbf{e}}(x) = \hat{\mathbf{D}}(x) \, \hat{\mathbf{N}}(x) \, \hat{\mathbf{v}} = \hat{\mathbf{a}}(x) \, \hat{\mathbf{v}} \tag{7}$$

where $\hat{\mathbf{a}}(x) = \hat{\mathbf{D}}(x) \, \hat{\mathbf{N}}(x)$ is the cross-section strain compatibility matrix.

According to Vlasov's warping description [6], strain fields $\gamma_y(x)$, $\gamma_z(x)$ and $\chi_x(x)$ are used to describe cross-section out-of-plane displacements. Indeed, displacement field $u_w(x, y, z)$ is defined as the linear combination of assigned 2D warping functions, defined over the cross-section area and collected in vector $\mathbf{M}_\eta(y, z) = \begin{Bmatrix} M_{\eta\,x}(y, z) & M_{\eta\,y}(y, z) & M_{\eta\,z}(y, z) \end{Bmatrix}$. These

are associated to torsion and shear along y- and z-directions, respectively, and, thus, are combined by means of the corresponding strain fields, assumed as warping parameters, $\boldsymbol{\eta}_s(x) = \left\{\chi_x(x) \quad \gamma_y(x) \quad \gamma_z(x)\right\}^T$, i.e.:

$$u_w(x,y,z) = \mathbf{M}_\eta(y,z)\,\boldsymbol{\eta}_s(x) \tag{8}$$

The warping functions $M_{\eta\,x}(y,z)$, $M_{\eta\,y}(y,z)$ and $M_{\eta\,z}(y,z)$ are determined according to the numerical procedure described in [20], which ensures the orthogonality conditions between rigid and warping displacements, as required by Equation (1). Examples of warping functions are depicted in Figure 2 for a S-shaped cross-section.

(a) (b) (c)

Figure 2: Warping functions for a S-shaped cross-section related to (a) torsion, $M_{\eta\,x}(y,z)$, (b) shear along y-axis, $M_{\eta\,y}(y,z)$, and (c) shear along z-axis, $M_{\eta\,z}(y,z)$

Accounting for the warping description in Equation (8), material strains are determined as:

$$\boldsymbol{\varepsilon}_m(x,y,z) = \hat{\boldsymbol{\alpha}}(y,z)\,\hat{\mathbf{e}}(x) \tag{9}$$

where $\hat{\boldsymbol{\alpha}}(y,z)$ is the cross-section compatibility operator. By enforcing the virtual work principle, the generalized section stresses, $\hat{\mathbf{s}}(x)$, are defined as:

$$\hat{\mathbf{s}}(x) = \int_{A(x)} \hat{\boldsymbol{\alpha}}^T(y,z)\,\boldsymbol{\sigma}_m(x,y,z)\,dA \tag{10}$$

with:

$$\hat{\mathbf{s}}(x) = \left\{N(x) \quad M_z(x) \quad T_y^p(x) \quad M_x^p(x) \quad M_y(x) \quad T_z^p(x) \quad B_x(x) \quad B_y(x) \quad B_z(x)\right\}^T \tag{11}$$

being $N(x)$ the axial stress, $M_z(x)$ and $M_y(x)$ the bending moments and $B_x(x)$, $B_y(x)$ and $B_z(x)$ the bi-moments, work-conjugate to $\zeta_x(x)$, $\zeta_y(x)$, $\zeta_z(x)$ [6, 13], i.e.:

$$B_k(x) = \int_{A(x)} M_{\eta\,k}(y,z)\,\sigma_{xx}(x,y,z)\,dA\,, \qquad \text{with} \quad k = x,y,z \tag{12}$$

Quantities $M_x^p(x)$, $T_y^p(x)$ and $T_z^p(x)$ are the *primary* torsional moment and shear stresses, each resulting as the sum of the corresponding standard stress, $M_x(x)$, $T_y(x)$ or $T_z(x)$, and bi-shear, $M_x^s(x)$, $T_y^s(x)$ or $T_z^s(x)$.

2.1.1 Derivation of the element governing equations

According to the displacement-based formulations [24], element equilibrium equations are derived from the stationarity of a Lagrangian functional, $\mathcal{L}\left[\mathbf{u}_m(x,y,z), \dot{\mathbf{u}}_m(x,y,z)\right]$, function of the displacements, $\mathbf{u}_m(x,y,z)$, and velocities, $\dot{\mathbf{u}}_m(x,y,z)$, and expressed as the difference of the element kinetic, $T\left[\dot{\mathbf{u}}_m(x,y,z)\right]$, and potential energy, $\Pi\left[\mathbf{u}_m(x,y,z)\right]$, that is:

$$\mathcal{L}\left[\mathbf{u}_m(x,y,z), \dot{\mathbf{u}}_m(x,y,z)\right] = T\left[\dot{\mathbf{u}}_m(x,y,z)\right] - \Pi\left[\mathbf{u}_m(x,y,z)\right] \tag{13}$$

Kinetic energy is expressed first in terms of cross-section velocities, $\dot{\hat{\mathbf{u}}}_s(x)$, and then in terms of nodal velocities, $\dot{\hat{\mathbf{u}}}$, as reported in details in [22]. Hence, it finally results as:

$$T\left(\dot{\hat{\mathbf{u}}}\right) = \frac{1}{2}\dot{\hat{\mathbf{u}}}^T \left(\mathbf{m}_r + \mathbf{m}_w\right) \dot{\hat{\mathbf{u}}} = \frac{1}{2}\dot{\hat{\mathbf{u}}}^T \mathbf{m}\, \dot{\hat{\mathbf{u}}} \tag{14}$$

where $\mathbf{m}_r$ and $\mathbf{m}_w$ are the element rigid and warping mass matrices related to the inertia effects due to $\mathbf{u}_r(x,y,z)$ and $u_w(x,y,z)$, respectively, while $\mathbf{m} = \mathbf{m}_r + \mathbf{m}_w$ is the total element consistent mass matrix.

Similarly, potential energy is expressed first in terms of cross-section quantities, $\hat{\mathbf{e}}(x)$ and $\hat{\mathbf{s}}(x)$, and then in terms of nodal quantities, $\hat{\mathbf{u}}$ and $\hat{\mathbf{p}}$, this latter collecting in vector $\mathbf{p}$ the standard forces and couples, $\mathbf{p}_{i/j}$ and $\mathbf{m}_{i/j}$, work-conjugate to $\mathbf{u}_{i/j}$ and $\theta_{i/j}$, and in vector β the additional generalized forces, β_i and β_j, work-conjugate to the warping DOFs, η_i and η_j, that is:

$$\hat{\mathbf{p}} = \left\{\mathbf{p}^T \quad \beta^T\right\}^T = \left\{\mathbf{p}_i^T \quad \mathbf{m}_i^T \quad \mathbf{p}_j^T \quad \mathbf{m}_j^T \quad \beta_i^T \quad \beta_j^T\right\}^T \tag{15}$$

Hence, it results:

$$\Pi\left(\hat{\mathbf{u}}\right) = \hat{\mathbf{u}}^T \left\{\hat{\mathbf{a}}_v^T \left[\int_L \hat{\mathbf{a}}^T(x)\, \hat{\mathbf{s}}(x)\, dx - \int_L \hat{\mathbf{N}}^T(x)\, \hat{\mathbf{q}}_s(x)\, dx\right] - \hat{\mathbf{p}} + \hat{\mathbf{p}}_{rq}\right\} \tag{16}$$

where $\hat{\mathbf{p}}_{rq}$ is the vector collecting the basic reaction forces due to distributed loads, $\hat{\mathbf{q}}_s(x)$. Under static loading conditions, the element equilibrium equations state that the term in brackets must equal the basic nodal force vector, $\hat{\mathbf{q}}$, work-conjugate to $\hat{\mathbf{v}}$ [20]. Hence, by considering Equations (14) and (16), expression of $\mathcal{L}$ in terms of nodal quantities is obtained as:

$$\mathcal{L}\left(\dot{\hat{\mathbf{u}}}, \hat{\mathbf{u}}\right) = \frac{1}{2}\dot{\hat{\mathbf{u}}}^T \mathbf{m}\, \dot{\hat{\mathbf{u}}} - \hat{\mathbf{u}}^T \left(\hat{\mathbf{a}}_v^T \hat{\mathbf{q}} - \hat{\mathbf{p}} + \hat{\mathbf{p}}_{rq}\right) \tag{17}$$

and the element governing equations are derived by enforcing its stationarity as:

$$\frac{d}{dt}\frac{\partial \mathcal{L}\left(\dot{\hat{\mathbf{u}}}, \hat{\mathbf{u}}\right)}{\partial \dot{\hat{\mathbf{u}}}} - \frac{\partial \mathcal{L}\left(\dot{\hat{\mathbf{u}}}, \hat{\mathbf{u}}\right)}{\partial \hat{\mathbf{u}}} = \frac{d}{dt}\frac{\partial T\left(\dot{\hat{\mathbf{u}}}\right)}{\partial \dot{\hat{\mathbf{u}}}} + \frac{\partial \Pi\left(\hat{\mathbf{u}}\right)}{\partial \hat{\mathbf{u}}} = \mathbf{0} \tag{18}$$

which gives the element equilibrium equations in the form:

$$\mathbf{m}\, \ddot{\hat{\mathbf{u}}} + \hat{\mathbf{a}}_v^T \hat{\mathbf{q}} + \hat{\mathbf{p}}_{rq} = \hat{\mathbf{p}} \tag{19}$$

Linearization of Equation (19) results as:

$$\mathbf{m}\, \Delta\ddot{\hat{\mathbf{u}}} + \hat{\mathbf{a}}_v^T\, \Delta\hat{\mathbf{q}} = \mathbf{m}\, \Delta\ddot{\hat{\mathbf{u}}} + \hat{\mathbf{a}}_v^T\, \hat{\mathbf{k}}_v\, \Delta\hat{\mathbf{v}} = \mathbf{m}\, \Delta\ddot{\hat{\mathbf{u}}} + \underbrace{\hat{\mathbf{a}}_v^T\, \hat{\mathbf{k}}_v\, \hat{\mathbf{a}}_v}_{\hat{\mathbf{k}}}\, \Delta\hat{\mathbf{u}} = \Delta\hat{\mathbf{p}} \tag{20}$$

where Δ indicates the quantity increment and $\hat{\mathbf{k}}$ is the element tangent stiffness matrix, being:

$$\hat{\mathbf{k}}_v = \frac{\partial \hat{\mathbf{q}}}{\partial \hat{\mathbf{v}}} = \int_L \hat{\mathbf{a}}^T(x) \frac{\partial \hat{\mathbf{s}}(x)}{\partial \hat{\mathbf{e}}(x)} \frac{\partial \hat{\mathbf{e}}(x)}{\partial \hat{\mathbf{v}}}\, dx = \int_L \hat{\mathbf{a}}^T(x) \frac{\partial \hat{\mathbf{s}}(x)}{\partial \hat{\mathbf{e}}(x)}\, \hat{\mathbf{a}}(x)\, dx \tag{21}$$

2.2 Simplified Warping Mixed Element

The SWME formulation considers an arbitrary number of nodes, n_w, located along the element axis (Figure 3), always including end nodes, i and j. At each node, three DOFs are added

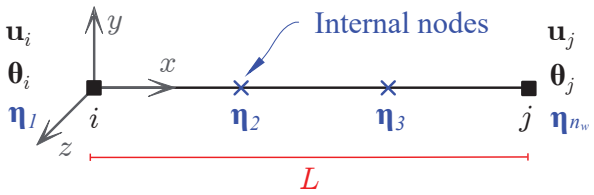

Figure 3: Standard (black) and warping (blue) nodal DOFs for the SWME model

and used to interpolate cross-section warping due to torsion and shear. These are collected in vector $\boldsymbol{\eta}_n = \{\eta_{x\,n} \quad \eta_{y\,n} \quad \eta_{z\,n}\}^T$, where subscript $n = 1, \ldots, n_w$ indicates the node number. Hence, the nodal displacement vector is written as:

$$\hat{\mathbf{u}} = \{\mathbf{u}^T \quad \boldsymbol{\eta}^T\}^T = \{\mathbf{u}_i^T \quad \boldsymbol{\theta}_i^T \quad \mathbf{u}_j^T \quad \boldsymbol{\theta}_j^T \quad \boldsymbol{\eta}_1^T \quad \boldsymbol{\eta}_2^T \quad \ldots \quad \boldsymbol{\eta}_{n_w}^T\}^T \tag{22}$$

The element rigid body motions are removed from the standard DOFs, $\mathbf{u}$, and vector $\mathbf{v}$, collecting the standard basic nodal displacements, is obtained as follows:

$$\mathbf{v} = \{u_j \quad \theta_{zi} \quad \theta_{zj} \quad \theta_{xj} \quad \theta_{yi} \quad \theta_{yj}\}^T = \mathbf{a}_v\,\mathbf{u} \tag{23}$$

being $\mathbf{a}_v$ the standard element compatibility matrix [18]. The total basic deformation displacement vector $\hat{\mathbf{v}}$ reads:

$$\hat{\mathbf{v}} = \{\mathbf{v}^T \quad \eta_{x\,1} \quad \eta_{y\,1} \quad \eta_{z\,1} \quad \ldots \quad \eta_{x\,n_w} \quad \eta_{y\,n_w} \quad \eta_{z\,n_w}\}^T = \{\mathbf{v}^T \quad \boldsymbol{\eta}^T\}^T \tag{24}$$

The SWME model follows a mixed beam formulation [25] where standard generalized cross-section stresses, $\mathbf{s}(x) = \{N(x) \quad M_z(x) \quad T_y(x) \quad M_x(x) \quad M_y(x) \quad T_z(x)\}^T$, are interpolated along the element axis, by enforcing the equilibrium conditions in strong form, i.e.:

$$\mathbf{s}(x) = \mathbf{b}(x)\,\mathbf{q} + \mathbf{s}_q(x) \tag{25}$$

being $\mathbf{q} = \{p_{x\,j} \quad m_{z\,i} \quad m_{z\,j} \quad m_{x\,j} \quad m_{y\,i} \quad m_{y\,j}\}^T$ the vector collecting the basic nodal forces work-conjugate to $\mathbf{v}$, $\mathbf{b}(x)$ the equilibrium matrix [23] and $\mathbf{s}_q(x)$ the generalized section stress vector due to distributed loads.

In addition, the warping displacement field $u_w(x, y, z)$ is interpolated. To this end, Benscoter's warping description is adopted [7], where, similarly to Equation (8), $u_w(x, y, z)$ is defined as the linear combination of warping functions, $\mathbf{M}_\eta(y, z)$. However, independent warping parameters, $\boldsymbol{\eta}_s(x) = \{\eta_x(x) \quad \eta_y(x) \quad \eta_z(x)\}^T$, are considered to describe warping variation along x. Hence, by exploiting the additional warping DOFs, $\eta_{x\,n}$, $\eta_{y\,n}$ and $\eta_{z\,n}$ at the element nodes, polynomial interpolation of fields $\eta_x(x)$, $\eta_y(x)$ and $\eta_z(x)$, respectively, is introduced and Equation (8) is written as:

$$u_w(x, y, z) = \sum_{n=1}^{n_w} N_n(x)\,\mathbf{M}_\eta(y, z)\,\boldsymbol{\eta}_n \tag{26}$$

being $N_n(x)$ the Lagrange polynomial shape function associated to node n.

The material strains $\boldsymbol{\varepsilon}_m(x,y,z)$ are, thus, determined as:

$$\begin{aligned}\boldsymbol{\varepsilon}_m(x,y,z) &= \boldsymbol{\alpha}(y,z)\,\mathbf{e}(x) + \boldsymbol{\alpha}_\zeta(y,z)\,\boldsymbol{\zeta}_s(x) + \boldsymbol{\alpha}_\eta(y,z)\,\boldsymbol{\eta}_s(x) = \\ &= \boldsymbol{\alpha}(y,z)\,\mathbf{e}(x) + \sum_{n=1}^{n_w}\left[\frac{\partial N_n(x)}{\partial x}\boldsymbol{\alpha}_\zeta(y,z) + N_n(x)\,\boldsymbol{\alpha}_\eta(y,z)\right]\boldsymbol{\eta}_n \end{aligned} \tag{27}$$

where three contributions are distinguished, the first related to rigid cross-section displacements and the others to warping. Vector $\mathbf{e}(x)$ collects the standard generalized cross-section strains work-conjugate to $\mathbf{s}(x)$ and matrix $\boldsymbol{\alpha}(y,z)$ is the compatibility operator, while vector $\boldsymbol{\zeta}_s(x) = \begin{Bmatrix}\zeta_x(x) & \zeta_y(x) & \zeta_z(x)\end{Bmatrix}^T$ contains the strain quantities assumed as equal to the derivatives of the warping parameters with respect to x (see also Equation (6)). Matrices $\boldsymbol{\alpha}_\zeta(y,z)$ and $\boldsymbol{\alpha}_\eta(y,z)$ are compatibility operators related to the warping field with size 3×3 [20].

The virtual work equivalence, enforced by alternatively assigning a virtual variation to the three fields composing $\boldsymbol{\varepsilon}_m(x,y,z)$ [20], leads to the definition of standard, $\mathbf{s}(x)$, and warping, $\mathbf{b}_w(x)$ and $\mathbf{t}_w(x)$, generalized cross-section stresses, that is:

$$\mathbf{s}(x) = \int_{A(x)} \boldsymbol{\alpha}^T(y,z)\,\boldsymbol{\sigma}_m(x,y,z)\,dA \tag{28}$$

$$\mathbf{b}_w(x) = \int_{A(x)} \boldsymbol{\alpha}_\zeta(y,z)^T\,\boldsymbol{\sigma}_m(x,y,z)\,dA, \qquad \mathbf{t}_w(x) = \int_{A(x)} \boldsymbol{\alpha}_\eta(y,z)^T\,\boldsymbol{\sigma}_m(x,y,z)\,dA \tag{29}$$

The latter are work-conjugate to $\boldsymbol{\zeta}_s(x)$ and $\boldsymbol{\eta}_s(x)$, respectively, and are equivalent to the *bi-moments* and *bi-shears* introduced in the EVDE model.

2.2.1 Derivation of the element governing equations

The element governing equations are derived from the stationarity of an extended Lagrangian functional, expressed as function of four independent fields, being these the material rigid displacements, $\mathbf{u}_r(x,y,z)$, total strains, $\boldsymbol{\varepsilon}_m(x,y,z)$, and stresses, $\boldsymbol{\sigma}_m(x,y,z)$, and warping displacement, $u_w(x,y,z)$, i.e.:

$$\mathcal{L}(\mathbf{u}_r, \boldsymbol{\varepsilon}_m, \boldsymbol{\sigma}_m, u_w, \dot{\mathbf{u}}_r, \dot{u}_w) = T(\dot{\mathbf{u}}_r, \dot{u}_w) - \Pi(\mathbf{u}_r, \boldsymbol{\varepsilon}_m, \boldsymbol{\sigma}_m, u_w) \tag{30}$$

where dependency of the quantities from spatial coordinates x, y and z is omitted for brevity. The kinetic energy is expressed first in terms of rigid cross-section velocities, $\dot{\mathbf{u}}_s(x)$, being $\mathbf{u}_s(x) = \begin{Bmatrix}u(x) & v(x) & \theta_x(x) & w(x) & \theta_y(x) & \theta_z(x)\end{Bmatrix}^T$, and then in terms of all nodal velocities, $\dot{\mathbf{u}}$ and $\dot{\boldsymbol{\eta}}$, following [23]. This is accomplished by accounting for Equation (26) and by expressing the rigid cross-section displacements and velocities in terms of nodal DOFs as follows:

$$\mathbf{u}_s(x) = \mathbf{N}_s(x)\,\mathbf{u} + \mathbf{N}_w(x)\,\boldsymbol{\eta} \qquad \text{and} \qquad \dot{\mathbf{u}}_s(x) = \mathbf{N}_s(x)\,\dot{\mathbf{u}} + \mathbf{N}_w(x)\,\dot{\boldsymbol{\eta}} \tag{31}$$

where $\mathbf{N}_s(x)$ and $\mathbf{N}_w(x)$ are the shape function matrices relating $\mathbf{u}_s(x)$ to the standard and warping nodal DOFs, $\mathbf{u}$ and $\boldsymbol{\eta}$, respectively. These are derived by using the unit load method, described in more detail in [23] for the EWME. Hence, the kinetic energy results as:

$$T\left(\dot{\mathbf{u}}, \dot{\boldsymbol{\eta}}\right) = \frac{1}{2}\dot{\mathbf{u}}^T\,\mathbf{m}_{rr}\,\dot{\mathbf{u}} + \dot{\mathbf{u}}^T\,\mathbf{m}_{rw}\,\dot{\boldsymbol{\eta}} + \dot{\boldsymbol{\eta}}^T\,\mathbf{m}_{wr}\,\dot{\mathbf{u}} + \frac{1}{2}\dot{\boldsymbol{\eta}}^T\,\left(\mathbf{m}^r_{ww} + \mathbf{m}_{ww}\right)\,\dot{\boldsymbol{\eta}} \tag{32}$$

where $\mathbf{m}_{rr}$, $\mathbf{m}_{rw}$, $\mathbf{m}_{wr}$ and $\mathbf{m}^r_{ww}$ are the element mass matrices associated to the generalized rigid cross-section velocity $\dot{\mathbf{u}}_s(x)$ and are defined as:

$$\mathbf{m}_{rr} = \int_L \mathbf{N}_s^T(x)\,\mathbf{m}_s(x)\,\mathbf{N}_s(x)\,dx \quad , \qquad \mathbf{m}_{rw} = \int_L \mathbf{N}_s^T(x)\,\mathbf{m}_s(x)\,\mathbf{N}_w(x)\,dx = \mathbf{m}_{wr}^T$$
$$\mathbf{m}^r_{ww} = \int_L \mathbf{N}_w^T(x)\,\mathbf{m}_s(x)\,\mathbf{N}_w(x)\,dx \tag{33}$$

being $\mathbf{m}_s(x)$ the standard rigid cross-section mass matrix [23], while $\mathbf{m}_{ww}$ is the element mass matrix associated to the warping velocity $\dot{u}_w(x,y,z)$ and is defined as:

$$\mathbf{m}_{ww} = \int_L \begin{bmatrix} N_1(x)\,\mathbf{m}_{sw}(x)\,N_1(x) & \dots & N_1(x)\,\mathbf{m}_{sw}(x)\,N_{n_w}(x) \\ \vdots & \ddots & \vdots \\ N_{n_w}(x)\,\mathbf{m}_{sw}(x)\,N_1(x) & \dots & N_{n_w}(x)\,\mathbf{m}_{sw}(x)\,N_{n_w}(x) \end{bmatrix} dx \tag{34}$$

being $\mathbf{m}_{sw}(x)$ the cross-section mass matrix associated to $\dot{u}_w(x,y,z)$, that results as:

$$\mathbf{m}_{sw}(x) = \int_{A(x)} \rho(x,y,z)\,\mathbf{M}_\eta^T(y,z)\,\mathbf{M}_\eta(y,z)\,dA \tag{35}$$

where $\rho(x,y,z)$ indicates the material density.

Similarly, the potential energy is expressed first in terms of the standard cross-section quantities, $\mathbf{u}_s(x)$, $\mathbf{e}(x)$ and $\mathbf{s}(x)$, and warping displacements, $u_w(x,y,z)$, and then in terms of standard cross-section strains and stresses, $\mathbf{e}(x)$ and $\mathbf{s}(x)$, and nodal DOFs, $\mathbf{u}$ and $\boldsymbol{\eta}$. Hence, it results:

$$\begin{aligned} \Pi(\mathbf{u},\mathbf{e},\mathbf{s},\boldsymbol{\eta}) &= \int_V \boldsymbol{\varepsilon}_m^T[\mathbf{e},u_w(\boldsymbol{\eta})]\,\boldsymbol{\sigma}_m(\boldsymbol{\varepsilon}_m)\,dV + \int_L \mathbf{s}^T\left\{\mathbf{e}[\mathbf{u}_s(\mathbf{u},\boldsymbol{\eta})]-\mathbf{e}\right\}dx + \\ &+ \Pi_{ext}[\mathbf{u},\boldsymbol{\eta},\mathbf{u}_s(\mathbf{u},\boldsymbol{\eta})] \end{aligned} \tag{36}$$

where $\Pi_{ext}[\mathbf{u},\boldsymbol{\eta},\mathbf{u}_s(\mathbf{u},\boldsymbol{\eta})]$ is the external load potential.

By considering Equations (32) and (36), expression of $\mathcal{L}$ results as:

$$\begin{aligned} \mathcal{L}\left(\mathbf{u},\mathbf{e},\mathbf{s},\mathbf{u}_w,\dot{\mathbf{u}},\dot{\boldsymbol{\eta}}\right) &= \frac{1}{2}\dot{\mathbf{u}}^T\,\mathbf{m}_{rr}\,\dot{\mathbf{u}} + \dot{\mathbf{u}}^T\,\mathbf{m}_{rw}\,\dot{\boldsymbol{\eta}} + \dot{\boldsymbol{\eta}}^T\,\mathbf{m}_{wr}\,\dot{\mathbf{u}} + \frac{1}{2}\dot{\boldsymbol{\eta}}^T\,\left(\mathbf{m}^r_{ww}+\mathbf{m}_{ww}\right)\,\dot{\boldsymbol{\eta}} + \\ &+ \int_V \boldsymbol{\varepsilon}_m^T[\mathbf{e},u_w(\boldsymbol{\eta})]\,\boldsymbol{\sigma}_m(\boldsymbol{\varepsilon}_m)\,dV + \int_L \mathbf{s}^T\left\{\mathbf{e}[\mathbf{u}_s(\mathbf{u},\boldsymbol{\eta})]-\mathbf{e}\right\}dx + \Pi_{ext}[\mathbf{u},\boldsymbol{\eta},\mathbf{u}_s(\mathbf{u},\boldsymbol{\eta})] \end{aligned} \tag{37}$$

and four element governing equations are derived, by assuming $\mathbf{u}$, $\mathbf{e}(x)$, $\mathbf{s}(x)$ and $\mathbf{u}_w$ as independent variables, that is by imposing the following four stationarity conditions:

$$\frac{d}{dt}\frac{\partial\mathcal{L}\left(\mathbf{u},\mathbf{e},\mathbf{s},\mathbf{u}_w,\dot{\mathbf{u}},\dot{\boldsymbol{\eta}}\right)}{\partial\dot{q}_h} - \frac{\partial\mathcal{L}\left(\mathbf{u},\mathbf{e},\mathbf{s},\mathbf{u}_w,\dot{\mathbf{u}},\dot{\boldsymbol{\eta}}\right)}{\partial q_h} = \frac{d}{dt}\frac{\partial T\left(\dot{\mathbf{u}},\dot{\boldsymbol{\eta}}\right)}{\partial\dot{q}_h} + \frac{\partial\Pi(\mathbf{u},\mathbf{e},\mathbf{s},\boldsymbol{\eta})}{\partial q_h} = \mathbf{0} \tag{38}$$

with $q_h \equiv \mathbf{u},\ \mathbf{e},\ \mathbf{s},\ \boldsymbol{\eta}$.

For $q_h \equiv \mathbf{e},\ \mathbf{s}$, the term related to the kinetic energy vanishes and the resulting equations are those holding for static loading conditions, that is the nonlinear material constitutive law and element compatibility enforced in weak form as:

$$\boldsymbol{\sigma}_m(x,y,z) = \hat{\boldsymbol{\sigma}}_m[\boldsymbol{\varepsilon}_m(x,y,z)] \tag{39}$$
$$\mathbf{v} = \int_L \mathbf{b}^T(x)\mathbf{e}(x)\,dx \tag{40}$$

By contrast, for $q_h \equiv \mathbf{u}, \boldsymbol{\eta}$ the dynamic equilibrium equations result, related to rigid and warping motions, respectively, and written as:

$$\mathbf{m}_{rr}\,\ddot{\mathbf{u}} + \qquad \mathbf{m}_{rw}\,\ddot{\mathbf{u}}_w + \qquad \mathbf{a}_v^T\mathbf{q} - \mathbf{p}_{rq} \qquad = \mathbf{p} \quad (41)$$

$$\mathbf{m}_{wr}\,\ddot{\mathbf{u}} + (\mathbf{m}_{ww}^r + \mathbf{m}_{ww})\;\ddot{\mathbf{u}}_w + \int_L \begin{bmatrix} \frac{\partial N_1(x)}{\partial x} \\ \dots \\ \frac{\partial N_{n_w}(x)}{\partial x} \end{bmatrix} \mathbf{b}_w(x)\,dx + \int_L \begin{bmatrix} N_1(x) \\ \dots \\ N_{n_w}(x) \end{bmatrix} \mathbf{t}_w(x)\,dx = \boldsymbol{\beta} \quad (42)$$

where $\mathbf{p}_{rq}$ is the vector collecting the basic reaction forces due to distributed loads, written considering only the twelve standard nodal components, while vectors $\mathbf{p}$ and $\boldsymbol{\beta}$ contain the element nodal forces work-conjugate to $\mathbf{u}$ and $\boldsymbol{\eta}$, respectively. These are arranged in the total nodal force vector $\hat{\mathbf{p}}$, resulting as:

$$\hat{\mathbf{p}} = \begin{Bmatrix} \mathbf{p}^T & \boldsymbol{\beta}^T \end{Bmatrix}^T = \begin{Bmatrix} \mathbf{p}_i^T & \mathbf{m}_i^T & \mathbf{p}_j^T & \mathbf{m}_j^T & \boldsymbol{\beta}_1^T & \boldsymbol{\beta}_2^T & \dots & \boldsymbol{\beta}_{n_w}^T \end{Bmatrix}^T \quad (43)$$

Linearization of Equations (41) and (42) is written in compact form as [23]:

$$\underbrace{\begin{bmatrix} \mathbf{m}_{rr} & \mathbf{m}_{rw} \\ \mathbf{m}_{wr} & \mathbf{m}_{ww}^r + \mathbf{m}_{ww} \end{bmatrix}}_{\mathbf{m}} \underbrace{\begin{Bmatrix} \Delta\ddot{\mathbf{u}} \\ \Delta\ddot{\boldsymbol{\eta}} \end{Bmatrix}}_{\Delta\ddot{\hat{\mathbf{u}}}} + \underbrace{\begin{bmatrix} \mathbf{k}_{rr} & \mathbf{k}_{rw} \\ \mathbf{k}_{wr} & \mathbf{k}_{ww}^r + \mathbf{k}_{ww} \end{bmatrix}}_{\mathbf{k}} \underbrace{\begin{Bmatrix} \Delta\mathbf{u} \\ \Delta\boldsymbol{\eta} \end{Bmatrix}}_{\Delta\hat{\mathbf{u}}} = \underbrace{\begin{Bmatrix} \Delta\mathbf{p} \\ \Delta\boldsymbol{\beta} \end{Bmatrix}}_{\Delta\hat{\mathbf{p}}} \quad (44)$$

and gives the definition of the total consistent element mass, $\mathbf{m}$, and stiffness matrix, $\mathbf{k}$. Similarly to $\mathbf{m}$, matrix $\mathbf{k}$ is composed by five contributions. First four, $\mathbf{k}_{rr}$, $\mathbf{k}_{rw}$, $\mathbf{k}_{wr}$ and $\mathbf{k}_{ww}^r$ are the element stiffness matrices associated to the generalized rigid cross-section displacement $\mathbf{u}_s(x)$ and are defined as:

$$\mathbf{k}_{rr} = \mathbf{a}_v^T\,\mathbf{f}^{-1}\,\mathbf{a}_v, \quad \mathbf{k}_{rw} = \mathbf{a}_v^T\,\mathbf{f}^{-1}\,\mathbf{b}_{sw}, \quad \mathbf{k}_{wr} = \mathbf{b}_{ws}\,\mathbf{f}^{-1}\,\mathbf{a}_v, \quad \mathbf{k}_{ww}^r = \mathbf{b}_{ws}\,\mathbf{f}^{-1}\,\mathbf{b}_{sw} \quad (45)$$

where $\mathbf{f}$ is the standard consistent element flexibility matrix [25] and $\mathbf{b}_{sw}$ and $\mathbf{b}_{ws}$ are the element warping compatibility and equilibrium matrices, respectively [18, 23]. While, $\mathbf{k}_{ww}$ is the element stiffness matrix associated to warping.

2.3 Enhanced Warping Mixed Element

The EWME formulation is the enhanced version of the SWME model. Indeed, a richer warping interpolation is performed in this case, by introducing an arbitrary number, m_w, of DOFs at each of the n_w element nodes. These are located at uniformly distributed points over the cross-section, as depicted in the examples of Figure 4. Hence, vector $\boldsymbol{\eta}_n$ collecting all DOFs, $u_{w\,nm}$, with $m = 1, \dots, m_w$, for node n, now reads as:

$$\boldsymbol{\eta}_n = \begin{Bmatrix} u_{w\,n1} & u_{w\,n2} & \dots & u_{w\,nm_w} \end{Bmatrix}^T \quad (46)$$

while nodal displacement vector $\hat{\mathbf{u}}$ is arranged as in Equation (22).

As opposed to the SWME, where warping profiles, $\mathbf{M}_\eta(y,z)$, over the cross-section are assigned, for the EWME, warping interpolation involves all three spatial dimensions. Hence, instead of Equation (26), this assumes:

$$u_w(x,y,z) = \sum_{n=1}^{n_w} N_n(x) \left[\sum_{m=1}^{m_w} M_m(y,z)\,u_{w\,nm} \right] = \sum_{n=1}^{n_w} N_n(x)\,\mathbf{M}_\eta(y,z)\,\boldsymbol{\eta}_n \quad (47)$$

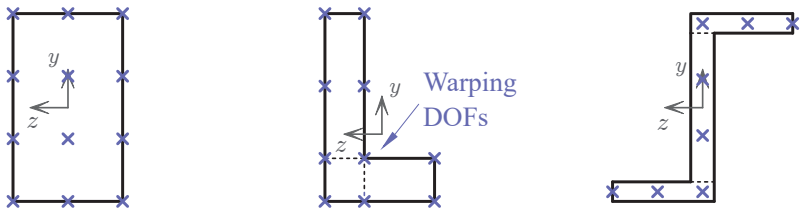

Figure 4: Examples of EWME warping DOFs for typical cross-sections at element node n

where $\mathbf{M}_\eta(y,z)$ is now a row vector containing 2D Lagrange polynomials $M_m(y,z)$ used to interpolate $u_w(x,y,z)$ over the cross-section plane.

The material strains, $\boldsymbol{\varepsilon}_m(x,y,z)$, are expressed in a similar fashion to Equation (27), i.e.:

$$\boldsymbol{\varepsilon}_m(x,y,z) = \boldsymbol{\alpha}(y,z)\,\mathbf{e}(x) + \sum_{n=1}^{n_w}\left[\frac{\partial N_n(x)}{\partial x}\boldsymbol{\alpha}_\zeta(y,z) + N_n(x)\,\boldsymbol{\alpha}_\eta(y,z)\right]\boldsymbol{\eta}_n \tag{48}$$

although matrices $\boldsymbol{\alpha}_\zeta(y,z)$ and $\boldsymbol{\alpha}_\eta(y,z)$ have, now, size $3 \times m_w$ and contain polynomials $M_m(y,z)$ and their derivatives with respects to y and z [20].

Generalized cross-section stresses playing the role of *bi-moments* and *bi-shears*, $\mathbf{b}_w(x)$ and $\mathbf{t}_w(x)$, are derived as in Equation (29) and all other fundamental relationships and governing equations are obtained through similar derivations performed for the SWME, that lead to formal identical expressions. Complete details of the element formulation are described in [23].

3 NUMERICAL APPLICATIONS

To validate and compare the performances of the adopted beam formulations, two numerical applications are considered. First application simulates the behavior of a steel L frame with beam and column having symmetric cross-sections and subjected to a base earthquake excitation. Second application reproduces the response of a RC U-shaped shear wall under similar loading conditions.

3.1 Steel L frame with flange continuity

The behavior of the steel frame depicted in Figure 5 is analyzed. The specimen is composed by a 4 m long column and 3 m long beam having same I-shaped cross-section geometry. Cross-section orientation is such that flange continuity is obtained at the beam-column connection joint (point C in the figure) and rigid and warping displacements are prevented at the ends of the frame (points A and E). Transverse displacement along y direction of point C is also restrained. Similar specimen was studied in [26, 27] under static loading conditions, while, here, dynamic response to ground acceleration is investigated. To this end, in addition to the mass of the frame, a lumped mass $M = 7645$ kg is considered, applied at mid-span of the beam (point D) and representing the mass of a typical slab supported by the frame. A small vertical eccentricity e is assumed between mass and centroidal axis of the beam, being equal to 0.05 m, that is half of the cross-section width.

Elasto-plastic material response is assumed. Thus, J2 plasticity model with linear kinematic hardening is adopted, with Young's modulus $E^s = 205000$ MPa, Poisson ratio $\nu^s = 0.3$, yielding stress $\sigma_y^s = 150$ MPa and hardening modulus $H_k^s = 0.01\,E^s$. Material density is assumed as equal to $\rho = 7850\,\text{kg/m}^3$.

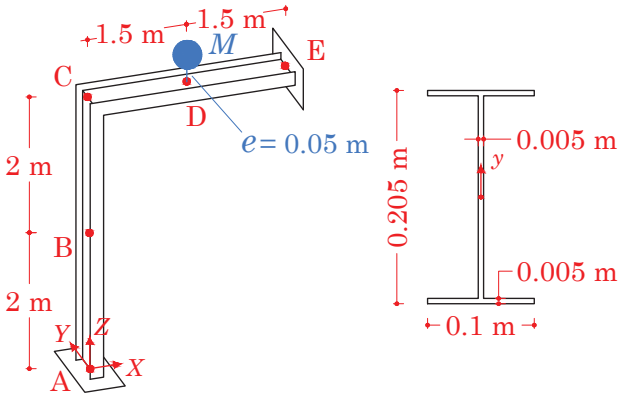

Figure 5: Geometry of the steel L frame with flange continuity.

A uniform mesh made of 10 and 14 FEs for beam and column, respectively, is used to model the frame. For the SWME and EWME, parabolic warping interpolation is assumed along the element axis, i.e. $n_w = 3$. Same order of interpolation is considered for torsional warping in the EVDE, while shear warping is assumed as linear (Equations (5) and (8)). Over the cross-section plane, EWME considers parabolic and cubic warping interpolation along web and flanges, respectively, and linear interpolation across the membrature thickness, i.e. $m_w = 28$, on the basis of the findings reported in [10, 18, 23, 20]. Same interpolation order is used to compute warping profile functions $\mathrm{M}_\eta(y, z)$, adopted in the EVDE and SWME.

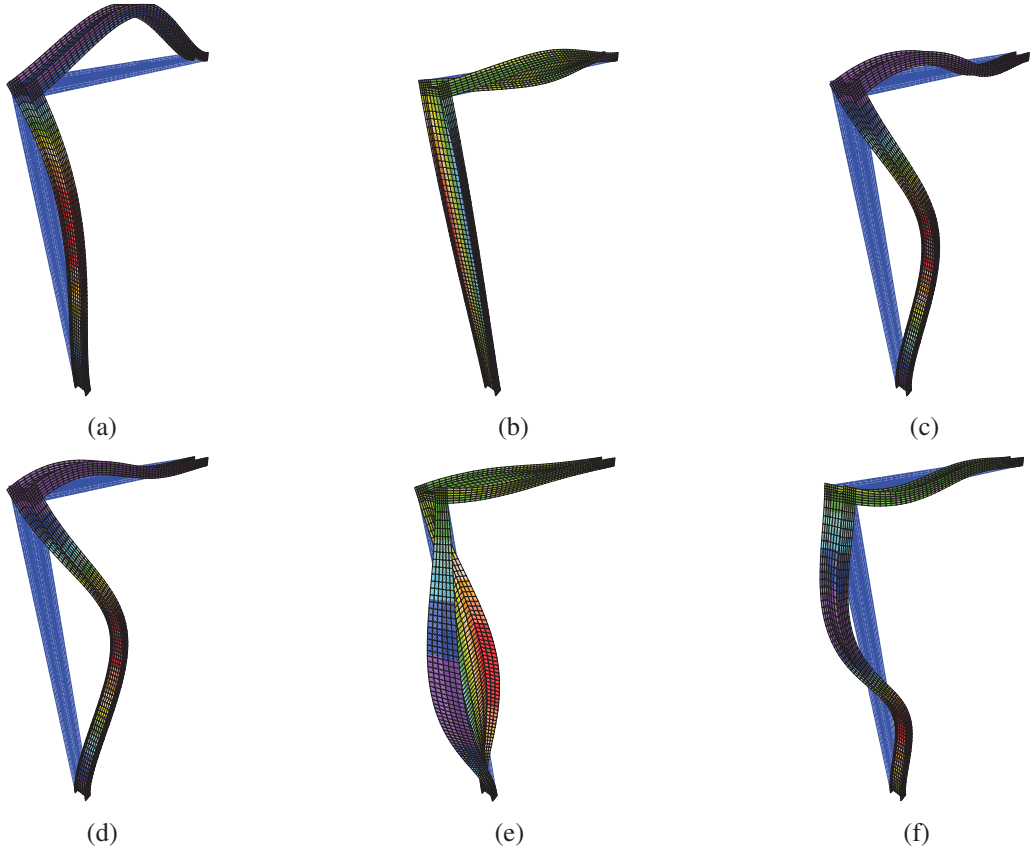

Figure 6: Steel L frame: deformed shape for mode (a) 1, (b) 2, (c) 3, (d) 4, (e) 5, (f) 6

Fiber discretization is used to compute nonlinear cross-section response, that is to evaluate cross-section resultant forces and stiffness. In this case, fibers are distributed according to the Gauss-Legendre rule, as exact integration of the element torsional stiffness is required to obtain the correct response of the frame. Fiber grid is arranged to have 6 fibers placed along web and flanges and 3 across the membrature thickness.

Table 1: Elastic circular frequency ω_i [rad/s] obtained for the L portal frame

FE type	Mode					
	1^{st} Flex.	1^{st} Tors.	2^{nd} Flex.	3^{rd} Flex.	2^{nd} Tors.	4^{th} Flex.
Shell	10.55	20.03	123.01	140.28	176.37	356.54
EWME	10.49	19.80	123.67	143.36	176.70	358.47
SWME	10.48	19.80	123.66	143.35	176.61	358.41
EVDE	10.49	19.87	123.68	143.37	176.28	358.54
Rigid section beam	10.48	9.07	123.64	143.33	84.70	358.27

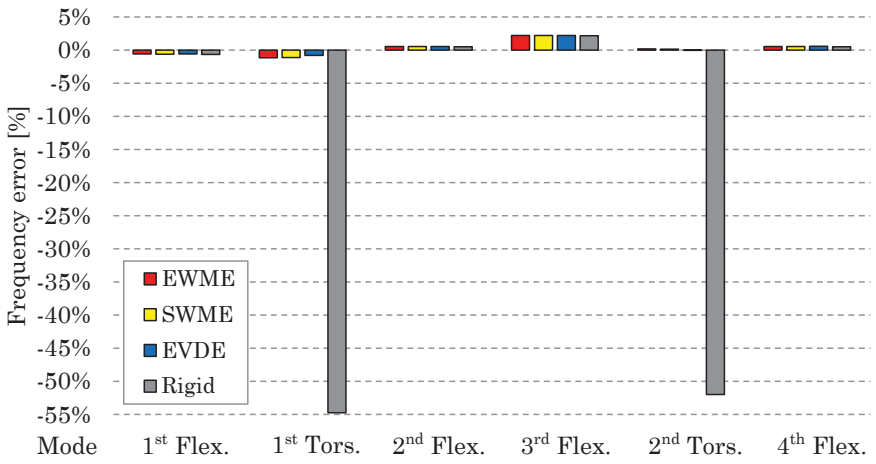

Figure 7: Steel L frame: circular frequency errors obtained with beam models with respect to the shell solution

For all models, damping ratio is set equal to 2% and introduced through Rayleigh method on the basis of the first two elastic frequencies of the frame [28]. These correspond to the first in plane flexural and torsional natural modes, respectively, as depicted in Figures 6(a) and 6(b). Indeed, Figure 6 shows the deformed shapes for the first 6 elastic modes obtained with a reference model made of 2268 4-node Discrete Kirchhoff Quadrilateral shell elements. The blue and colored configurations indicate the undeformed and deformed shapes, respectively. The circular frequencies ω_i are reported in Table 1 and are compared with the values obtained from the adopted enhanced beam models and with a standard beam model assuming rigid cross-section. For this latter, cross-section torsional inertia is computed according to the thin-walled beam theory and results equal to $J = \kappa_t \, I_\rho$, being I_ρ the cross-section polar inertia and $\kappa_t = 0.001153$ the correction coefficient. Figure 7 shows the solution differences in terms of percentage error for ω_i with respect to the reference results. As shown, all enhanced beam formulations give similar results that perfectly agree with the shell solution. By contrast, the standard beam model provides incorrect frequency values for the torsional modes. Indeed, this model neglects warping and, thus, warping restraints at the boundaries. Moreover, due to the particular orientation, the

end cross-sections of beam and column that meet at the joint C undergo equal warping profile. As a result, when beam twists, warping of the end cross-section at C produces warping in the column, which twists as well (see, for instance, Figure 6(e)). As opposed to the standard model, in the enhanced beam formulations, the additional nodal warping DOFs placed at the nodes permit to correctly account for boundary restraints. Moreover, mesh connectivity ensures warping continuity between column and beam and, thus, the correct warping transmission at the joint C.

The frame dynamic response is also investigated by applying to the frame the ground acceleration history depicted in Figure 8(a), and considering both linear elastic and elasto-plastic constitutive behavior. Peak ground acceleration results equal to $0.4167\,\mathrm{g}$, where g indicates the gravity acceleration. Figure 8(b) shows the resulting Fourier transform and, thus, indicates the frequency content of the acceleration signal. In the same figure, the green dotted vertical line indicates the value of the first torsional natural frequency of the frame. Ground acceleration is assumed to act in the direction Y transverse to the frame plane. Newmark method [28] is adopted for time integration of the structure global equilibrium equations, with coefficients $\beta = 0.25$ and $\gamma = 0.5$ and time step set equal to 0.001 s.

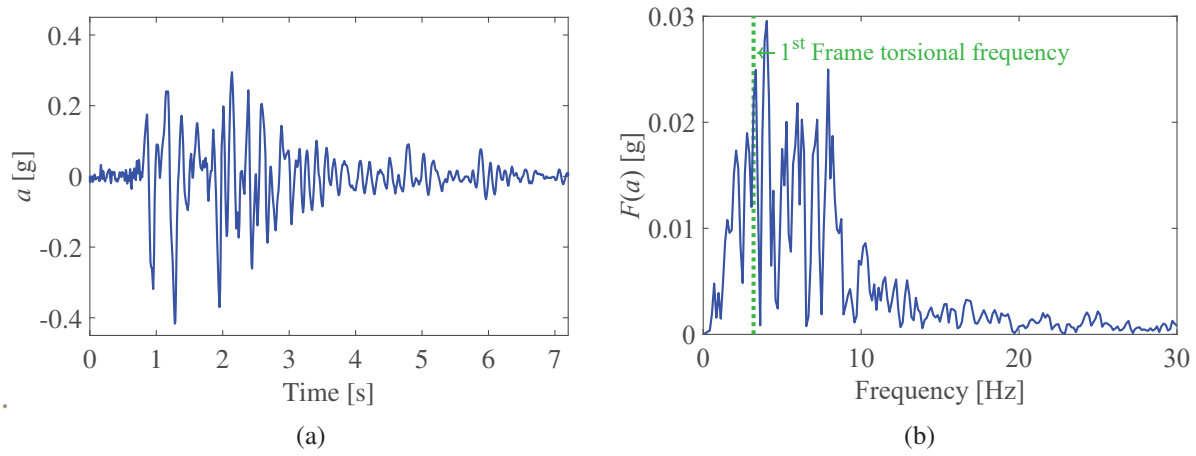

Figure 8: Base excitation signal: ground acceleration (a) history and (b) Fourier transform

Although mass eccentricity, e, is small, the applied ground acceleration mainly induces torsional deformation of the beam and, due to warping continuity, torsion is transmitted to the column. By contrast, transverse flexural deformation are mainly limited to the beam, as expected, given the assumed boundary restraints. Figure 9 plots the time-evolution of (a) the torsional rotation, θ_x^B, of the column mid-height cross-section, (b) the torsional rotation, θ_x^D, and (c) transverse displacement, v^D, of the beam mid-span cross-section, respectively, under the assumption of linear elastic material. Solid black curves represent the reference solutions obtained with the shell FEs. Red, yellow and blue curves refer to those obtained with the EWME, SWME and EVDE models, respectively. Finally, dotted dark gray curves indicate the response obtained with the standard beam formulations. As observed in the modal decomposition analysis, standard beam model, not considering the boundary warping restraints, provides a significantly more flexible response, as opposed to all enhanced models that perfectly agree with the reference response. In addition, standard model does not account for warping transmission at the joint and, thus, gives null rotations for the column (horizontal line at zero in Figures 9(a), as opposed to the enhanced beam models that correctly capture the column torsional deformation.

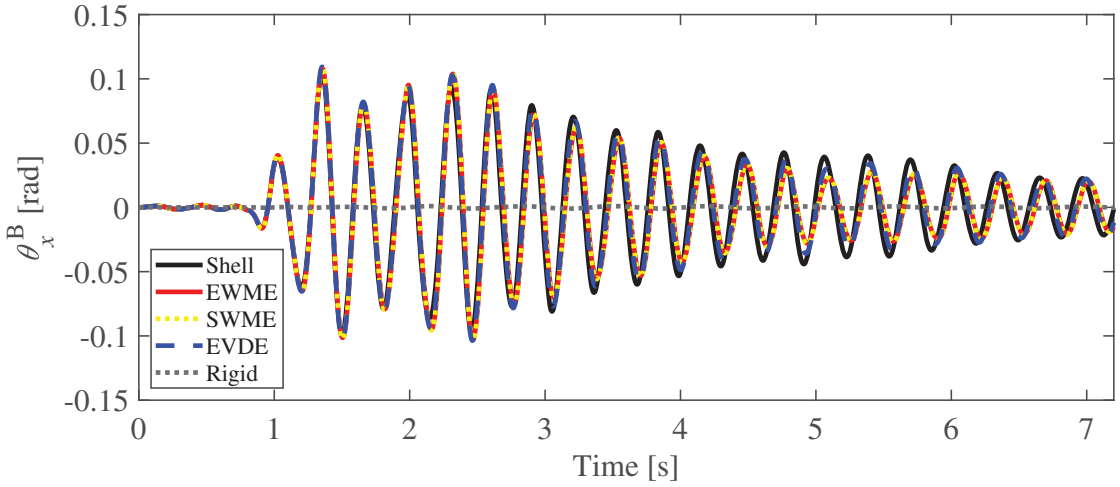

(a)

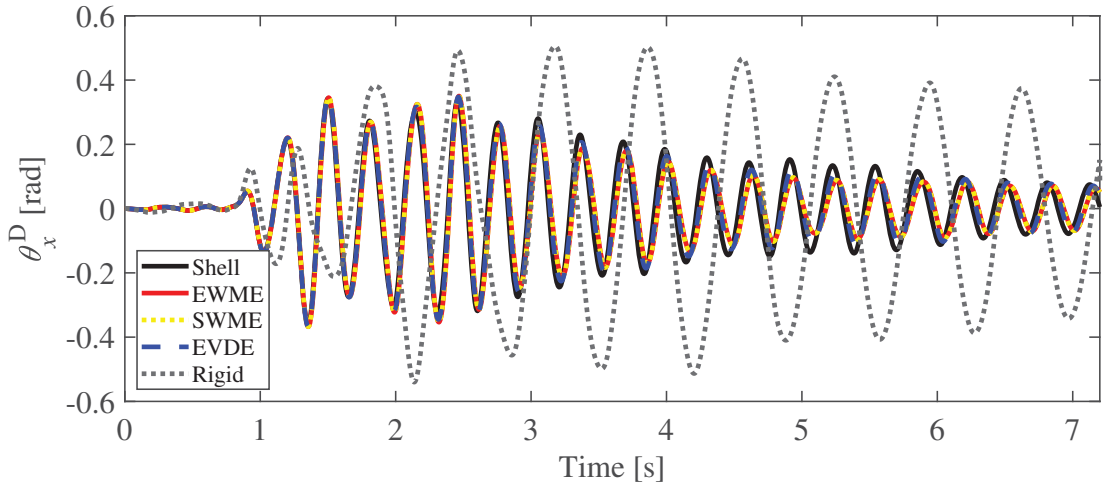

(b)

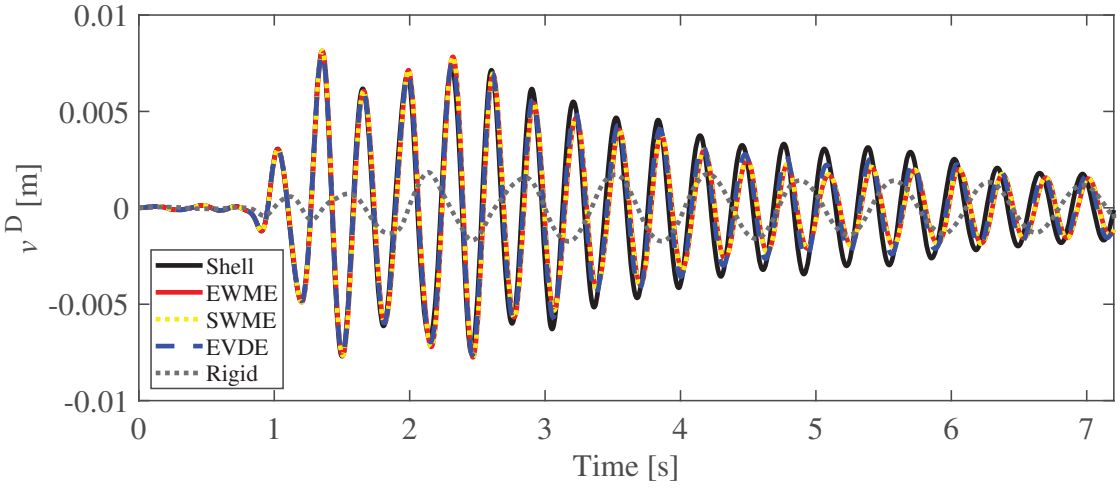

(c)

Figure 9: Linear elastic response of the steel L frame: time history of (a) the torsional rotation of the column at mid-height (point B), (b) torsional rotation and (c) transverse displacement of the beam at mid-span (point D)

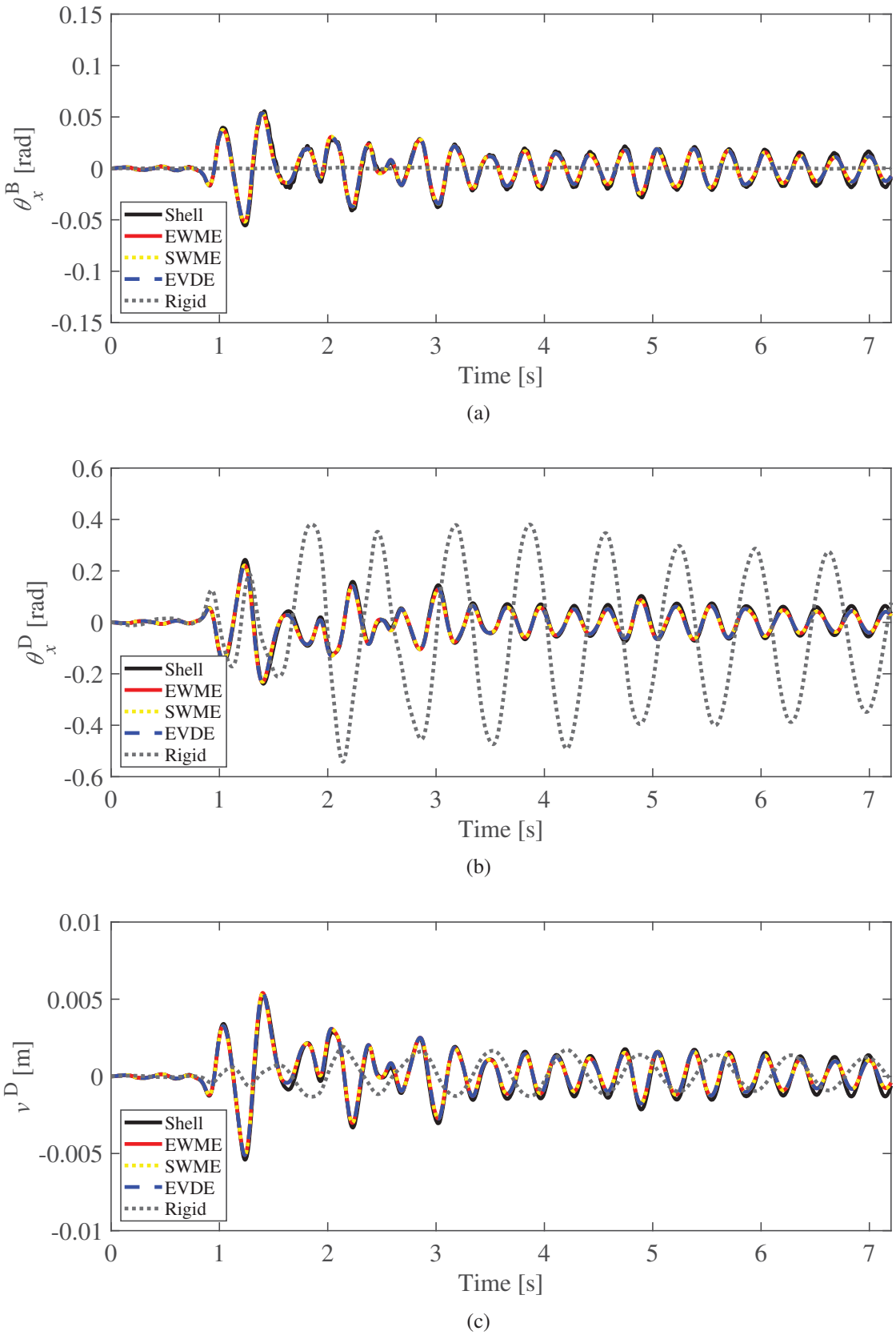

Figure 10: Nonlinear response of the steel L frame: time history of (a) the torsional rotation of the column at mid-height (point B), (b) torsional rotation and (c) transverse displacement of the beam at mid-span (point D)

Similar results are plotted in Figure 10 for elasto-plastic material response, showing that all enhanced beam formulations correctly simulate the evolution of the plastic effects in the material. Indeed, due to warping constraints, torsion of the members induces significant shear-lag effects and, thus, when ground acceleration reaches the peak value, at almost $1.3\,\mathrm{s}$, axial stress exceeds material yield stress, at both ends and mid-height of the beam. Consequently, plastic strains affect the remaining part of the time-history response. As opposed to the beam model formulations accounting for warping, the standard beam model does not capture shear-lag and shows yielding of the material caused by severe torsional shear stresses acting in the cross-section plane.

Fourier transforms of the beam and column rotation histories, θ_x^B and θ_x^D, are plotted in Figure 11, for (a-b) linear elastic and (c-d) nonlinear material response, respectively. These confirm that main frequency content of the response is associated to torsional deformation mode of the frame. First torsional frequency of the frame is indicated by the green dotted vertical lines.

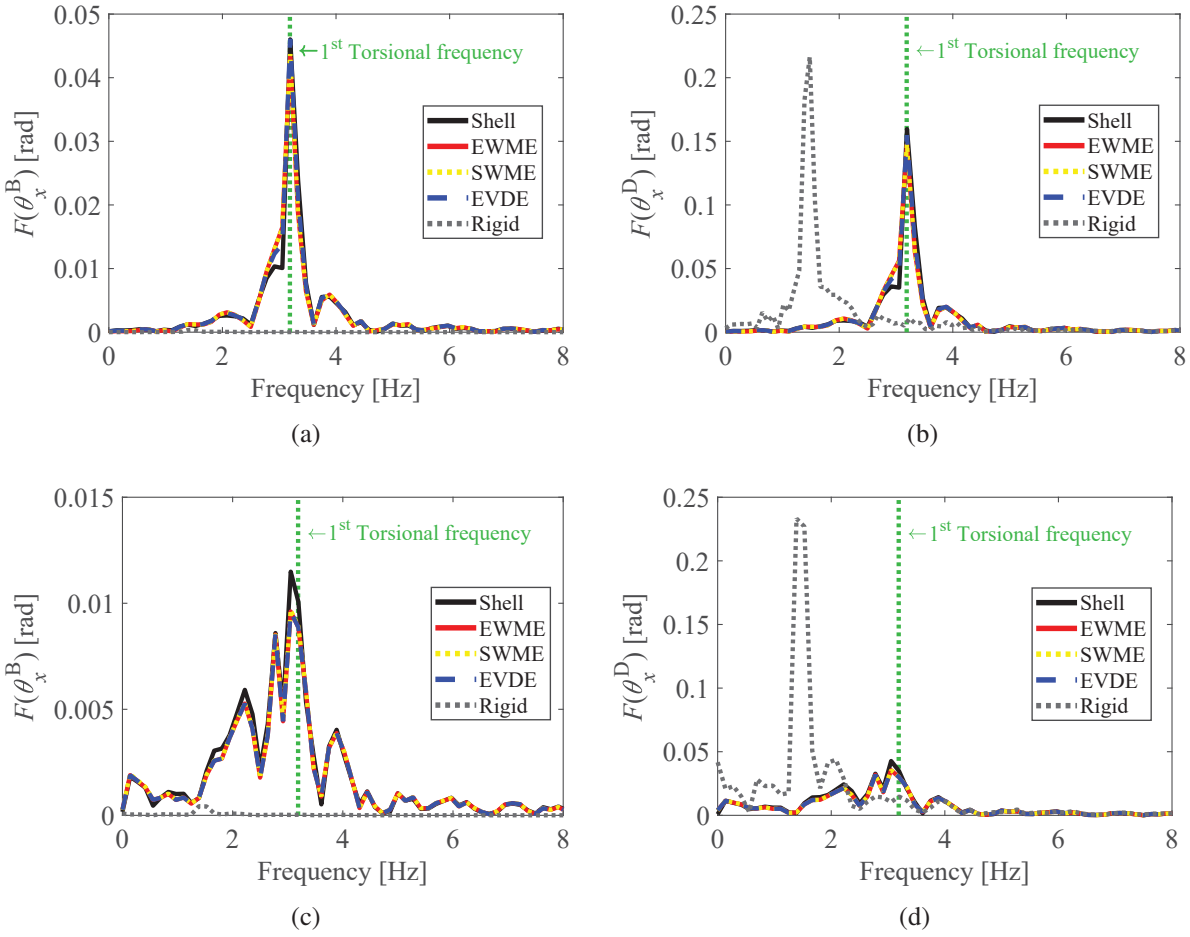

Figure 11: Steel L frame: Fourier transform of the torsional rotation of (a-c) the column mid-height (point B) and (b-d) beam mid-span cross-section (point D), for (a-b) linear elastic and (c-d) nonlinear material response

3.2 RC U-shaped shear wall

To investigate the performances of the presented enhanced beam models describing the interaction between warping and damaging mechanisms, the response of the RC U-shaped shear wall in Figure 12 is analyzed under dynamic loadings. Same specimen was experimental tested

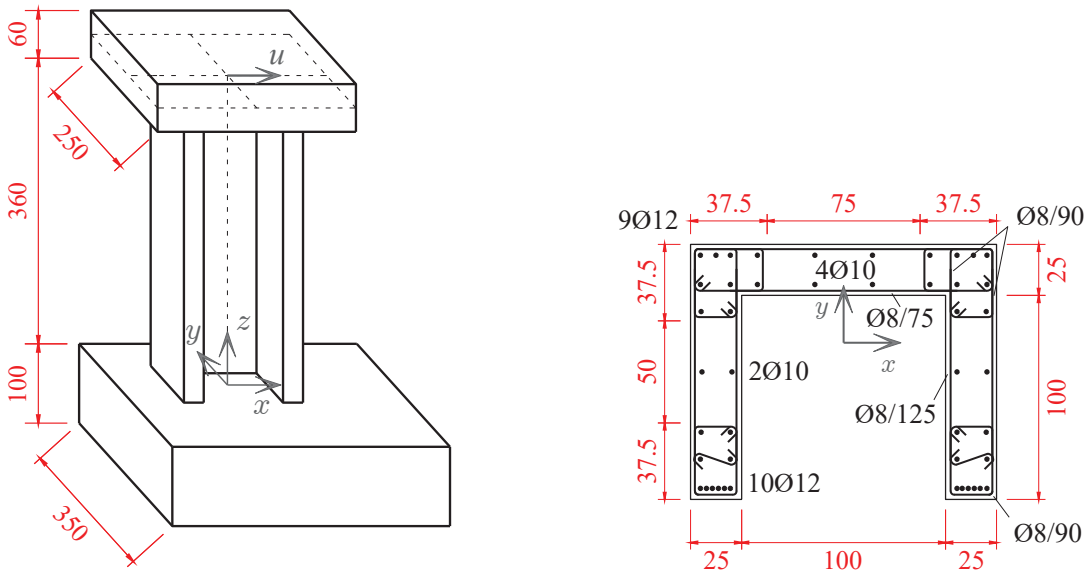

(a) Specimen geometry (b) Wall cross-section

Figure 12: RC U-shaped shear wall: (a) specimen and (b) cross-section geometry (dimensions in cm)

by Pegon et al. [29] under cyclic transverse loads applied at the top slab, while ground acceleration is considered, here, as base excitation, i.e. the same signal reported in Figure 8 but scaled so that peak ground acceleration results equal to $0.8334\,\mathrm{g}$. This is assumed to act in the x direction, parallel to the wall web.

In addition to the weight of the top slab, the wall is vertically loaded by a constant compression force equal to $2000\,\mathrm{kN}$. As a result, a lumped mass $M = 203969\,\mathrm{kg}$ is applied at the top of the wall (at $z = 3.90\,\mathrm{m}$), representing the mass of the slab and that of the additional vertical load. Concrete density is assumed as equal to $\rho = 2548.42\,\mathrm{kg/m^3}$.

The wall is modeled as a vertical cantilever, where square slabs are assumed to fully prevent warping deformations of the bottom and top cross-sections. A uniform mesh made of 4 FEs is used. For the SWME and EWME, parabolic warping interpolation is assumed along the element axis, i.e. $n_w = 3$. Over the cross-section plane, EWME considers cubic warping interpolation along web and flanges and linear interpolation across the membrature thickness, i.e. $m_w = 24$. Same interpolation order is used to compute warping profile functions $\mathbf{M}_\eta(y, z)$, adopted in the EVDE and SWME.

A cross-section fiber discretization is defined so that 9 fibers are placed along web and flanges and 3 across the membrature thickness, while concrete response is reproduced by adopting the damage-plastic model proposed in [18]. Table 2 lists the material parameters, being σ_t and σ_c the uniaxial plastic limit stress in tension and compression, respectively, H_k and H_i the kinematic and isotropic hardening moduli, respectively, Y_{0t} and Y_{0c} the damage thresholds in tension and compression, respectively, k_t, a_t, k_c, a_c and β parameters governing the damage evolution. Young's modulus and Poisson ratio are assumed as equal to $E = 28000\,\mathrm{MPa}$ and $\nu = 0.25$, respectively. The Giuffrè-Menegotto-Pinto model [30] describes the behavior of the steel reinforcing bars, with $E^s = 200\,000\,\mathrm{MPa}$, $\sigma_y^s = 540\,\mathrm{MPa}$ and $b = 1.0\%$ being the Young's modulus, plastic yield strength and ratio between hardening and elastic stiffness, respectively. The transition coefficient R from the elastic to the plastic state required in the model results from the following parameters: $R_0 = 20$, $a_1 = 18.5$ and $a_2 = 0.15$ and no isotropic hardening is assumed.

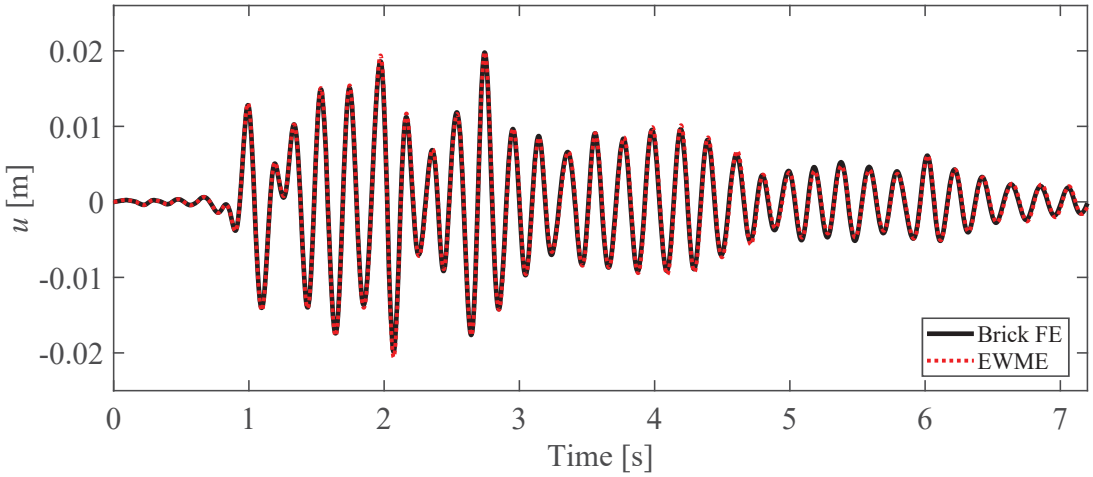

(a)

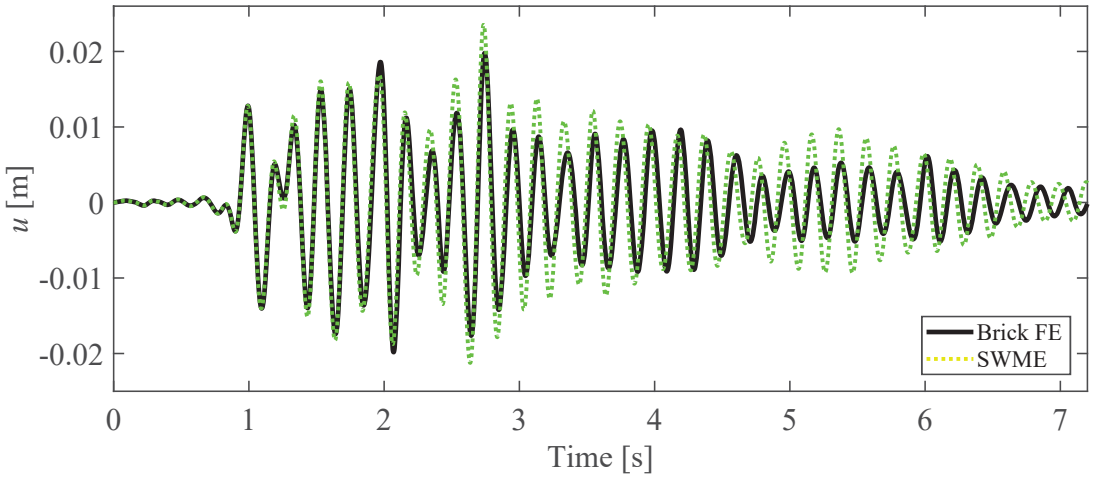

(b)

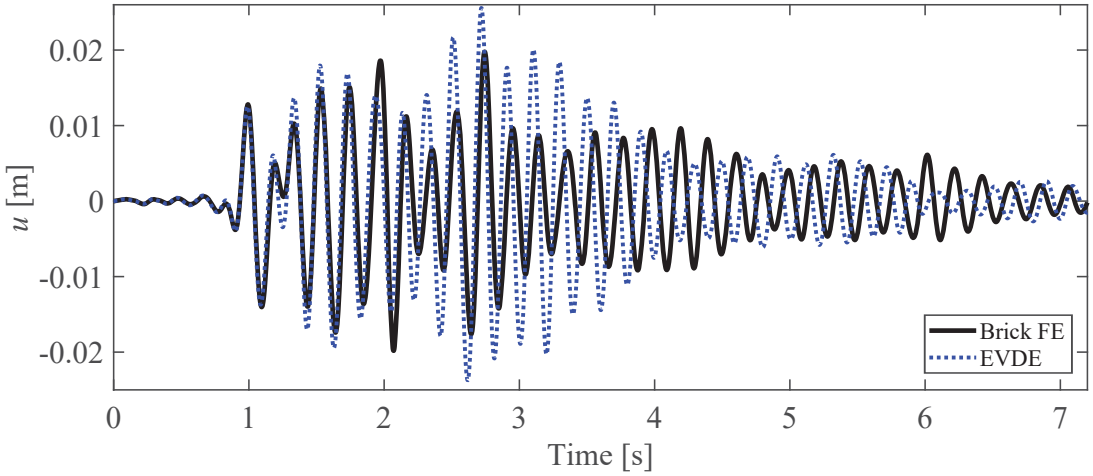

(c)

Figure 13: Linear elastic response of the RC U-shaped shear wall: time history of the transverse displacement u, along x, of the top slab obtained with (a) EWME (red dotted curve), (b) SWME (green dotted curve) and (c) EVDE (blue dotted curve), compared with the reference brick FE solution (black curves)

Table 2: Material parameters for concrete model in RC U-shaped wall.

σ_t	σ_c	H_k	H_i	Y_{0t}	k_t	a_t	Y_{0c}	k_c	a_c	β
3.3 MPa	30 MPa	$0.8\,E$	$0.001\,E$	$6.7\,10^{-5}$	$2.0\,10^{-5}$	0.8	$4.0\,10^{-4}$	$2.8\,10^{-3}$	0.8	0.5

Damping ratio is set equal to 2% and introduced through Rayleigh method [28] on the basis of the first two elastic frequencies of the frame and Newmark method [28] is adopted for time integration of the structure global equilibrium equations, with coefficients $\beta = 0.25$ and $\gamma = 0.5$ and time step set equal to 0.001 s.

Figure 13 shows the evolution of the transverse displacement u, along x, of the top slab, under linear elastic material behavior, for (a) EWME model (red dotted curve), (b) SWME model (green dotted curve) and (c) EVDE model (blue dotted curve). Each response is compared with a reference solution (black curve) obtained with a FE model made by 24480 8-node bricks.

As opposed to the steel portal frame analyzed in Section 3.1, in this test, the asymmetric geometry of the wall cross-section induces significant coupling between shear/bending in the x-z plane and torsional behavior. As a consequence, only the most sophisticated EWME model is able to correctly capture the shear/torsional warping interaction and provide the same solution as that obtained by the brick 3D model. The SWME provides a correct response only for the first 2 s of the history, while it slightly overestimates the wall horizontal displacement for the remaining part. Worse results are obtained with the EVDE, whose response also shows a significant overestimation of the maximum displacements occurring during oscillations. However, if compared with the solution provided by a standard beam model assuming rigid cross-sections, that obtained with the SWME results significantly more accurate, proving that this model can be considered as a good compromise between more sophisticated, but onerous, formulations and simpler, but less demanding, approaches. The standard beam solution is plotted in Figure 14 as gray dotted curve. For this model, shear areas in the x and y directions are set equal to $A_t^x = 0.4286\,A$ and $A_t^y = 0.7142\,A$, being A the cross-section area, while torsional inertia is assumed as $J = 0.05495\,I_\rho$, being I_ρ the cross-section polar inertia.

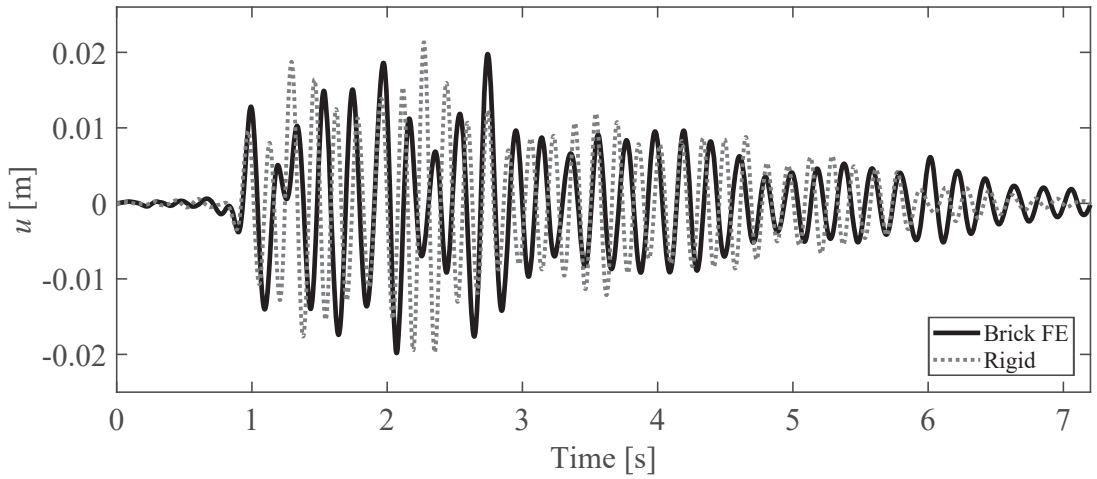

Figure 14: Linear elastic response of the RC U-shaped shear wall: time history of the transverse displacement u, along x, of the top slab obtained with reference brick FE (black curve) and standard beam (gray dotted curve) solutions

Different trend is observed for nonlinear material behavior. Figure 15 shows the displacement time histories along x of the top slab, obtained by considering the nonlinear response of concrete and steel. Figure 15(a) compares the solution obtained with the EWME (red curve) with the linear elastic response provided by the brick FE model (gray curve). When ground acceleration reaches the peak value, at almost 1.3 s, the wall significantly damages at the base, without collapsing. As a result, structural response with lower frequency content is observed compared to the linear elastic behavior. As expected, higher peak displacements occur in the first part of the history, around the peak acceleration, while lower amplitude oscillations are shown in the remaining part.

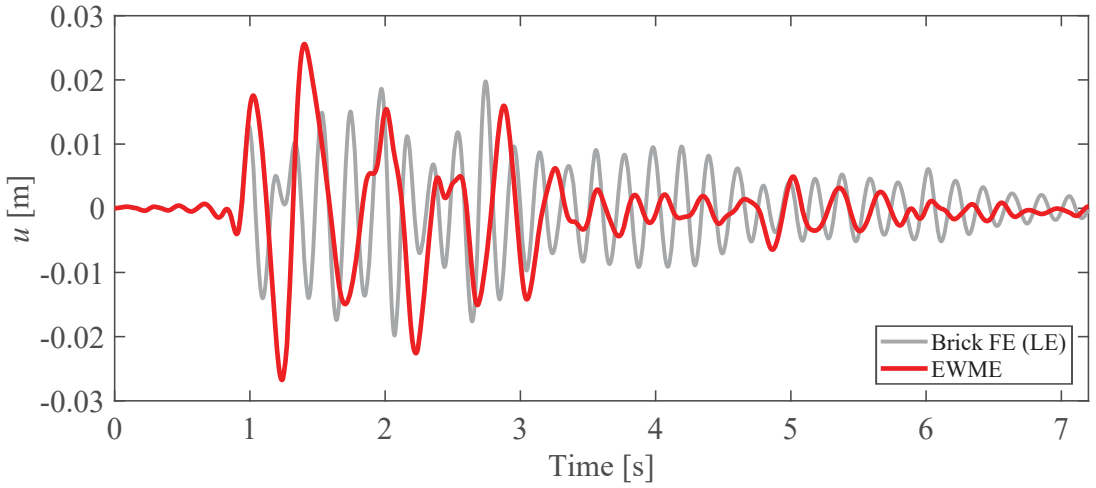

(a)

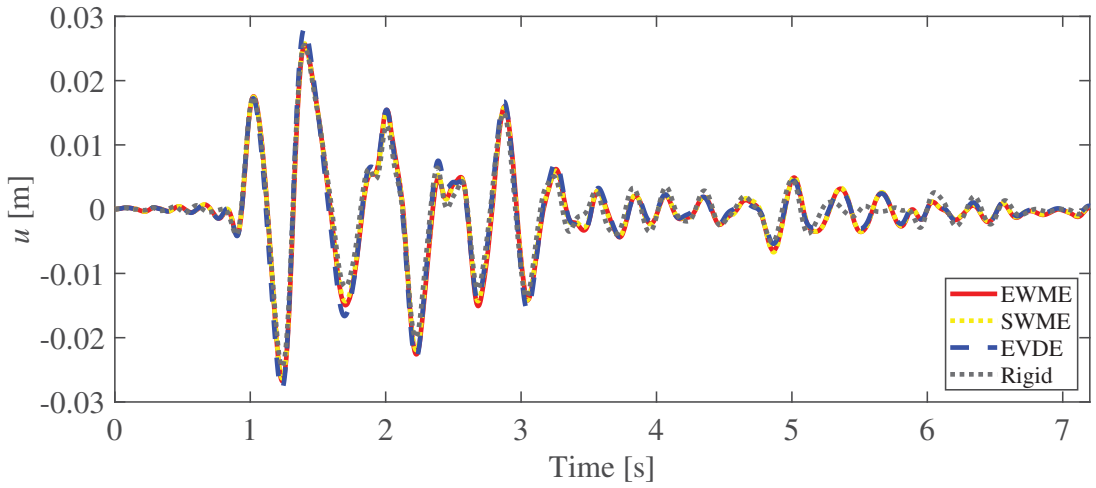

(b)

Figure 15: Nonlinear response of the RC U-shaped shear wall: time history of the transverse displacement u, along x, of the top slab obtained with (a) EWME (red curve) and (b) SWME (yellow dotted curve), EVDE (blue dashed curve) and standard beam (gray dotted curve)

In this case, all beam formulations, including the standard model, are able to correctly reproduce the wall response, as shown in Figure 15(b). This compares solutions obtained with the other beam models (SWME as yellow dotted curve, EVDE as blue dashed curve and standard beam as gray dotted curve) with the EWME results (red curve). Indeed, after damaging, wall behavior is

mainly governed by the nonlinear hinge that forms at the base and, although shear contribution is not negligible, warping effects become less important.

Fourier transforms of the displacement histories are plotted in Figures 16, using same curve styles of Figure 15. Green dotted vertical line indicates the value of the first elastic natural frequency of the wall involving shear/bending in the x direction, coupled with torsion.

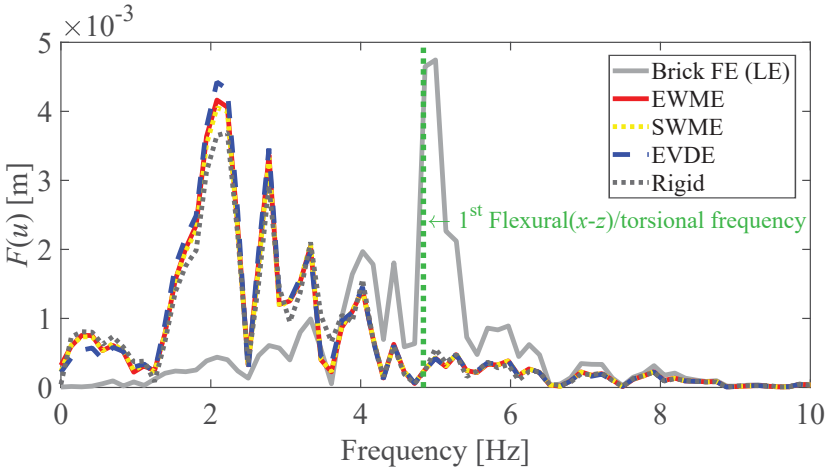

Figure 16: RC U-shaped shear wall: Fourier transform of the transverse displacement histories of the top slab

This plot confirms that, for the nonlinear behavior, natural modes of the wall that are excited by the seismic action are associated to lower frequencies, compared to the linear elastic response, as damage reduces the stiffness of the structure.

The values of the first four elastic circular frequencies ω_i obtained from all models are reported in Table 3.

Table 3: Elastic circular frequency ω_i [rad/s] obtained for the RC U-shaped shear wall

FE type	Mode			
	1^{st} Flex.(y-z)	1^{st} Flex.(x-z)/Tors.	1^{st} Axial.	2^{nd} Flex.(x-z)/Tors.
Brick	28.24	30.39	181.91	465.05
EWME	29.03	31.02	185.08	490.81
SWME	29.01	31.60	185.08	510.73
EVDE	29.18	32.61	185.08	542.53
Rigid section beam	28.86	35.32	185.08	205.75

4 CONCLUSIONS

- This paper presented three beam FE formulations for the analysis of frame structures subjected to dynamic shear and torsional actions. These are derived by extending to the dynamic analysis previously proposed enriched models, where kinematic description includes shear and torsional cross-section warping and, thus, coupling between axial/bending and shear/torsional stress components.

- More sophisticated EWME model considers a detailed two-level warping displacement field interpolation. By contrast, SWME model considers pre-defined profile functions

to describe warping variation over the cross-section and interpolates warping along the element axis only, by means of independent quantities, according to Benscoter's theory. Similar assumptions are made in the EVDE model, but warping axis variation is directly linked to torsional curvature and shear strains, according to Vlasov's theory.

- Numerical analyses performed on the steel L frame showed that, when torsional effects dominate the response, standard beam formulations based on rigid cross-section assumption fail in reproducing the correct structural behavior. By contrast, all three enhanced FEs result highly accurate and are preferable to higher order shell/brick FE models for the analysis of large scale structures, due to the lower computational cost these require. This is particularly true for the simplest model of the three, EVDE, which, however, gives satisfactory results only for open symmetric cross-section geometries, as proven in [20]. For closed and/or un-symmetric profiles, SWME model is the best alternative of the set, as this involves a lower number of additional nodal DOFs than EWME.

- Numerical analyses performed on the RC U-shaped shear wall confirm the findings observed for the steel L frame. Linear elastic response predicted with EWME model perfectly matches that evaluated with the 3D brick FE model. Good approximation is also obtained with the SWME model. Instead, major discrepancies are detected with the EDVE formulation, as a consequence of the non-symmetric cross-section geometry. However, tests also showed that nonlinear phenomena due to onset of damage can significantly modify the structural response, making the warping effects less important. As a result, correct structural response may be obtained also with simpler models and even standard formulations.

REFERENCES

[1] P. Di Re, E. Lofrano, D. Addessi, A. Paolone, Enhanced beam formulation with cross-section warping under large displacements. *Proceedings of the XXIV AIMETA Conference 2019. Lecture Notes in Mechanical Engineering*, 1217–1229, Springer, Cham, 2020. DOI: 10.1007/978-3-030-41057-5_99.

[2] N.L. Rizzi, V. Varano, The effects of warping on the postbuckling behaviour of thin-walled structures. *Thin-Walled Structures*, **49**(9), 1091–1097, 2011, DOI: 10.1016/j.tws.2011.04.001.

[3] N.L. Rizzi, V. Varano, S. Gabriele, Initial postbuckling behavior of thin-walled frames under mode interaction. *Thin-Walled Structures*, **68**, 124–134, 2013, DOI: 10.1016/j.tws.2013.03.004.

[4] Rinchen, G.J Hancock, K.J.R. Rasmussen, Geometric and material nonlinear analysis of thin-walled members with arbitrary open cross-section. *Thin-Walled Structures*, **153**, 106783, 2020.

[5] M. Brunetti, E. Lofrano, A. Paolone, G. Ruta, Warping and Ljapounov stability of non-trivial equilibria of non-symmetric open thin-walled beams. *Thin-Walled Structures*, **86**, 73–82, 2015, DOI: 10.1016/j.tws.2014.10.004.

[6] V.Z. Vlasov, *Thin-walled elastic beams*. National Technical Information Service, 1984.

[7] S.U. Benscoter, A theory of torsion bending for multicell beams. *Journal of Applied Mechanics*, **21**(1), 25–34, 1954.

[8] S.W. Lee, Y.H. Kim, A new approach to the finite element modelling of beams with warping effect. *International Journal for Numerical Methods in Engineering*, **24**(12), 2327–2341, 1987.

[9] K. Yoon, Y. Lee, P.-S. Lee, A continuum mechanics based 3-D beam finite element with warping displacements and its modeling capabilities. *Structural Engineering and Mechanics*, **43**(4), 411–437, 2012.

[10] P. Di Re, D. Addessi, F.C. Filippou, 3D beam-column finite element under non-uniform shear stress distribution due to shear and torsion. *VII European Congress on Computational Methods in Applied Sciences and Engineering (ECCOMAS 2016)*, Crete Island, Greece, June 5-10, 2016, **3**, 4467–4480, 2016, DOI: 10.7712/100016.2125.9035.

[11] P. Di Re, D. Addessi, A mixed 3D corotational beam with cross-section warping for the analysis of damaging structures under large displacements. *Meccanica*, **53**(6), 1313–1332, 2018, DOI: 10.1007/s11012-017-0749-3.

[12] R.E. Erkmen, M. Mohareb, Torsion analysis of thin-walled beams including shear deformation effects. *Thin-Walled Structures*, **44**(10), 1096–1108, 2006, DOI: 10.1016/j.tws.2006.10.012.

[13] R. El Fatmi, Non-uniform warping including the effects of torsion and shear forces. Part I: A general beam theory. *International Journal of Solids and Structures*, **44**, 5912–5929, 2007.

[14] P. Ceresa, L. Petrini, R. Pinho, Flexure-shear fiber beam-column elements for modeling frame structures under seismic loading - State of the art. *Journal of Earthquake Engineering*, **11**, 46–88, 2007, DOI: 10.1080/13632460701280237.

[15] D. Camotim, C. Basaglia, N. Silvestre, GBT buckling analysis of thin-walled steel frames: a state-of-the-art report. *Thin-Walled Structures*, **48**(10-11), 726–743, 2010.

[16] A. Genoese, A. Genoese, A. Bilotta, G. Garcea, A generalized model for heterogeneous and anisotropic beams including section distortions. *Thin-Walled Structures*, **74**, 85–103, 2014.

[17] A. Kagermanov, P. Ceresa, Fiber-section model with an exact shear strain profile for two-dimensional RC frame structures. *Journal of Structural Engineering*, **143**(10), 04017132, 2017.

[18] P. Di Re, D. Addessi, F.C. Filippou, Mixed 3D Beam Element with Damage Plasticity for the Analysis of RC Members under Warping Torsion. *Journal of Structural Engineering*, **144**(6), 04018064, 2018, DOI: 10.1061/(ASCE)ST.1943-541X.0002039.

[19] L. Librescu, O. Song, *Thin-walled composite beams: theory and application*. Springer Science & Business Media, 2006.